HELSINKI INSTITUTE OF PHYSICS INTERNAL REPORT SERIES

HIP-2008-06

Primordial Isocurvature Perturbation in Light of CMB and LSS Data

Vesa Muhonen

Helsinki Institute of Physics
P.O.Box 64, FIN-00014 University of Helsinki, Finland

ACADEMIC DISSERTATION
To be presented, with the permission of the Faculty of Science of the University of Helsinki, for public criticism in the Small Auditorium (E204) of Physicum, Gustaf Hällströmin katu 2a, on 27th of August 2008, at 12 o'clock.

Helsinki 2008

ISBN 978-952-10-3724-5 (printed version)
ISBN 978-952-10-3725-2 (pdf version)
ISSN 1455-0563
http://ethesis.helsinki.fi
Yliopistopaino
Helsinki 2008

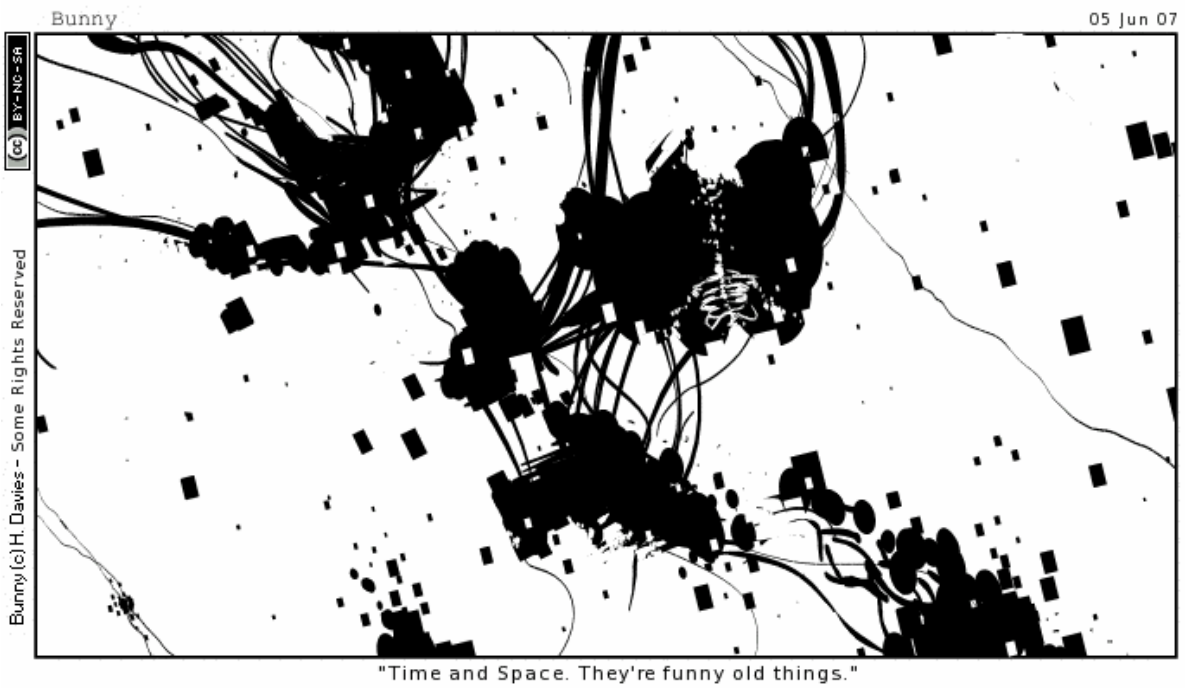
Bunny
05 Jun 07
BY-NC-SA
Bunny(c)H.Davies - Some Rights Reserved
"Time and Space. They're funny old things."

Contents

V. Muhonen: Primordial Isocurvature Perturbation in Light of CMB and LSS Data, University of Helsinki, 2008, 68 p. + appendices, Helsinki Institute of Physics, Internal Report Series, HIP-2008-06.
ISSN 1455-0563, ISBN 978-952-10-3724-5 (printed version), ISBN 978-952-10-3725-2 (pdf version).
INSPEC classification: A9870V, A9880B, A9880D.
Keywords: cosmology, early universe, CMB theory, isocurvature, parameter estimation, Markov chain Monte Carlo.

Abstract

The increased accuracy in the cosmological observations, especially in the measurements of the comic microwave background, allow us to study the primordial perturbations in greater detail. In this thesis, we allow the possibility for correlated isocurvature perturbations alongside the usual adiabatic perturbations.

Thus far the simplest six parameter ΛCDM model has been able to accommodate all the observational data rather well. However, we find that the 3-year WMAP data and the 2006 Boomerang data favour a non-zero non-adiabatic contribution to the CMB angular power spectrum. This is primordial isocurvature perturbation that is positively correlated with the primordial curvature perturbation.

Compared with the adiabatic ΛCMD model we have four additional parameters describing the increased complexity in the primordial perturbations. Our best-fit model has a 4% non-adiabatic contribution to the CMB temperature variance and the fit is improved by $\Delta\chi^2 = 9.7$. We can attribute this preference for isocurvature to a feature in the peak structure of the angular power spectrum, namely, the widths of the second and third acoustic peak.

Along the way, we have improved our analysis methods by identifying some issues with the parameterisation of the primordial perturbation spectra and suggesting ways to handle these. Due to the improvements, the convergence of our Markov chains is considerably improved. The change of parameterisation has an effect on the MCMC analysis because of the change in priors. We have checked our results against this and find only marginal differences between our parameterisations.

Acknowledgments

The research work for this thesis has been carried out at the Physics Department of the University of Helsinki and the Helsinki Institute of Physics. I wish to thank all the numerous people here for creating an enjoyable environment for study and research.

I wish to acknowledge the Graduate School in Astronomy and Space Physics, the Finnish Cultural Foundation, Magnus Ehrnrooth Foundation, Emil Aaltonen Foundation and Finnish Academy of Science and Letters for financial support and CSC – Scientific Computing Ltd. for computational resources. Parts of this work have been done under the EU 6th Framework Marie Curie Research and Training network "UniverseNet" (MRTN-CT-2006-035863).

First, I wish to thank my supervisors, professor Kari Enqvist and docent Hannu Kurki-Suonio. Your guidance and excellent physical insight has always been readily available during all my years at the university, as has your patience during those very same years. I'm grateful to the referees of the thesis, Filippo Vernizzi and Tuomas Lappi, for constructive criticism, good suggestions and their flexibility on the schedule.

Jussi, your enthusiasm about science and life in general made you a excellent collaborator and a good friend. Besides, it was nice to work with someone with a similarly non-standard daily rhythm. I also wish to thank my latest collaborator, Reijo, it has been a pleasure.

Masi, Janne, Ari, Timo and Suvi, thank you for your friendship during all this time, you have kept me (at least moderately) sane while working on this. I have truly enjoyed your company, on and especially off the department. My friends and colleagues, Sami, Vappu, Lotta, Gerasimos, Teppo, Touko and many others at the department, thank you for the many pleasant discussions we have had over the years, occasionally even on physics.

All physics and no play makes Vesa a dull boy. To counteract such a case I can count on my friends at the Kashima-Shinryū Helsinki shibu to provide me a way to take my mind away from physics and focus all my attention on something completely different yet equally enticing. Ari, Peter, Sami, Jari, Nuutti, Valtteri and Petteri, training with you has given me more than I could have imagined back when I first contacted Ari about joining in.

Finally, I wish to express my most sincere gratitude to my family, both my little sisters and my wonderful parents who, in the end, have made all this possible.

Vesa Muhonen
Helsinki, August 2008

List of Included Papers

The three articles [1, 2, 3] included in this thesis are:

1. J. Valiviita and V. Muhonen, "Correlated adiabatic and isocurvature CMB fluctuations in the wake of WMAP," Phys. Rev. Lett. **91** (2003) 131302 [arXiv:astro-ph/0304175].

2. H. Kurki-Suonio, V. Muhonen and J. Valiviita, "Correlated Primordial Perturbations in Light of CMB and LSS Data," Phys. Rev. D **71** (2005) 063005 [arXiv:astro-ph/0412439].

3. R. Keskitalo, H. Kurki-Suonio, V. Muhonen and J. Valiviita, "Hints of Isocurvature Perturbations in the Cosmic Microwave Background?," JCAP **0709** (2007) 008 [arXiv:astro-ph/0611917].

Author's Contribution

The idea for the first paper and the additions to CAMB to produce correlated isocurvature models came from J. Väliviita. I wrote the additions to parallelise the code to multiprocessor environment. The later optimisations and parameter selection and analysis was done conjointly.

In the second paper we moved to proper Monte Carlo analysis. I was responsible for the creation of the MCMC chains. The results and the issues arising from using MCMC methods in correlated modes were analysed jointly between all authors.

In the last paper the generation of the chains was done by R. Keskitalo. Like previously, all the analysis was done jointly by all the authors.

Chapter 1

Introduction

In less than two decades, the increase in the quantity and especially the quality of the available cosmological data has been nothing but truly remarkable. Over time, cosmology has evolved from pondering general questions about the universe and not getting precise answers to a true physical science where studying detailed issues gives detailed answers. From these bits of details we can then try to understand the whole universe.

Today the most important source of data is the cosmic microwave background radiation (CMB) and specifically the small, one part in a hundred thousand, temperature anisotropies we observe in it. This radiation originates from the time when the universe was only a few hundred thousand years old. Having travelled essentially undisturbed ever since, it is an excellent observable of the early universe. The most interesting part, the small temperature anisotropies, mirror the small perturbations in the energy density of the universe at the time.

While the CMB data is currently the most accurate data available, perhaps the most surprising or even the most influential bit of data comes from the supernovae. This data seems to imply that the current expansion of the universe is accelerating instead of decelerating which is the expected scenario [4]. Including this effect in the evolution of the universe is almost trivial, as shown in section 2.2.2, but understanding it is definitely not and remains one of the most important open questions in cosmology today.

An additional set of data that is currently expanding rapidly is that from the galaxy redshift surveys which track the three-dimensional distribution of galaxies [5]. This large-scale structure (LSS) data comes from a much later period and on smaller scales than the CMB. Partially due to this, it has not yet reached the same level of accuracy as the CMB data we have today. Nonetheless, it is an important addition to the CMB data and it is the combined set of CMB and LSS data that we use in this thesis.

From all the available data, something we can call the concordance model, or the standard model, of cosmology has arisen. The overall geometry of the universe seems to be flat, or at least nearly so. The normal baryonic matter covers only about five percent of the total energy density of the universe while the rest is in form of dark matter (dm) and dark energy (de).

The dark matter constitutes roughly a quarter of the energy density. The existence of dark matter

is suggested by several different observations from the rotation velocities of galaxies to the recent observation of the Bullet cluster [6]. Theoretically, such matter is not a huge issue as we simply require the existence of a species of particles which do not interact with photons. Candidates for such are readily available, for example, in the supersymmetric extensions of the standard model of particle physics [7].

The dark matter can be separated into hot and cold dark matter (hdm/cdm) depending on whether or not the particles are relativistic at the time they decouple from thermal equilibrium. A well-known example of hot dark matter are the neutrinos, which are expected to be massive. However, having only hot dark matter causes problems with galaxy formation and thus can not be the whole story [8]. On the upside, because of the effect on the large-scale structure, it is possible to obtain good constraints on the total mass of the three neutrino species from large-scale observations [9]. Due to the problems associated with the hot dark matter and because the detailed properties of the dark matter are not the focus of this thesis, we assume the dark matter to be cold dark matter.

The remaining 70 % of the energy density is in the form the dark energy. This is the component responsible for the accelerated expansion of the universe. In order to achieve this, the dark energy must possess the curious property of negative pressure. The simplest form of dark energy is just Einstein's cosmological constant Λ as introduced in section 2.1.2. Unlike the case of dark matter, there is currently no clear understanding what the dark energy fundamentally is. Also, the observational evidence is not unequivocally supportive of the dark energy [10]. Because of these theoretical and observational issues, there is currently some activity to explain the dark energy away altogether [11].

The paradigm of cosmological inflation is currently the favourite candidate for generating the small perturbations in the energy density in the first place. There are countless models of inflation around, but they all share the basic idea that the energy density of the universe is dominated by one or more scalar fields during the first few fractions of a second. The simplest models are the ones with a single field and they have been able to accommodate the observations admirably. However, these models can produce one type of perturbation only, namely, the adiabatic type. In this thesis, we consider a more generic situation where we allow the possibility of an isocurvature type of perturbation in addition to the adiabatic one.

This thesis is structured as follows. In chapter 2 we review the evolution of the smooth backround universe and introduce the inflationary paradigm. In chapter 3 we look into the perturbations away from the smooth background universe and the generation of the CMB and its anisotropies. In chapter 4 we introduce the tools for analysing the available data and present our main results. In chapter 5 we present the concluding remarks and some outlook for the future.

Notation

In this thesis we use the natural unit system, wherein the speed of light, Planck's constant and Boltzmann's constant are set to unity:

$$c = 1, \qquad \hbar = 1 \qquad \text{and} \qquad k_{\mathrm{B}} = 1. \tag{1.1}$$

The Planck mass is given by

$$M_{\mathrm{Pl}}^{-2} = 8\pi G. \tag{1.2}$$

The overdot is derivative with respect to the coordinate time, prime with respect to the conformal time and subscript comma with respect to the coordinate or field:

$$\dot{f} = \frac{\partial f}{\partial t}, \qquad f' = \frac{\partial f}{\partial \eta}, \qquad f_{,i} = \frac{\partial f}{\partial x^i}, \qquad \text{and} \qquad V_{,\varphi} = \frac{\partial V}{\partial \varphi}. \tag{1.3}$$

The indices run as usual, Roman letters denote the spatial coordinates and run from one to three while Greek letter run from zero to three:

$$i, j, k, \ldots \in \{1, 2, 3\} \qquad \text{and} \qquad \mu, \nu, \ldots \in \{0, 1, 2, 3\}. \tag{1.4}$$

Chapter 2

The Smooth Universe

Observing the world on the "human" scale of one meter and one second it seems a rather complicated place. Especially so if one desires to describe the world accurately in terms of mathematics and physical laws. However, taking our considerations to large enough scales, the physics becomes relatively simple and we can follow the evolution of the universe as a whole while disregarding all processes on small scales.

In this chapter we review the evolution of the universe that is described as a smooth expanding spacetime the matter content of which is described by an ideal fluid. This description is not quite satisfying in explaining all of the features in the early universe. To rectify these issues we introduce the model of inflation. While not the only suggested solution it is by far the most studied one and thus the one we shall concentrate on.

2.1 Friedmann-Lemaître Cosmologies

Based on observations such as the distribution of faint radio sources [12] and especially the CMB [13], we know that the universe is isotropic around us to a very high degree on several scales. The most stringent limit comes from the CMB where the anisotropy, disregarding the dipole component induced by our movement with respect to the last scattering surface (lss), is at 10^{-5} level. In addition to the fact that the universe is isotropic around us, we assume that this holds everywhere and an observer would see a similarly isotropic universe around him anywhere. This assumption, known as the cosmological or Copernican principle, asserts that the universe is isotropic everywhere from which it follows that the universe must also be homogeneous everywhere.

The above statement on isotropy and homogeneity is of course an approximation as our immediate environment is highly inhomogeneous and anisotropic. The solar system and the galaxy we are in are definitely nether isotropic nor homogeneous. Only when we observe scales of 100 Mpc[1] and larger are isotropy and homogeneity valid approximations.

Also, since the universe is not infinitely old, we can only observe it up to a finite distance and

[1] In comparison our galaxy is some 0.03 Mpc in diameter and the typical distance between galaxies is roughly 1 Mpc.

this part is referred to as the observable universe. There is nothing to suggest that our observable universe comprises the whole universe or even any significant fraction of it. Thus our assumption of isotropy and homogeneity has an upper limit as well since we have no way of knowing the properties of the universe on scales larger that we can actually observe. Fortunately, this is not a problem, because even if the universe should happen to be highly inhomogeneous on the largest scales, due to causality any effects on our observable part would happen on time scales comparable to the current age of the universe. So it would be an issue only if we were to follow the evolution of the universe to a distant future, which we are not interested in this thesis.

The proper theory to describe the universe as a whole is Einstein's general relativity (GR). The first person to suggest a solution to the Einstein equations that describes an expanding spacetime was the Russian mathematician Alexander Friedmann in 1922. Independently of him the Belgian priest and astronomer Georges Lemaître published similar ideas in 1927 (see [14] for extended discussion and the original references). Hence the class of models describing an expanding universe is referred to as the Friedmann-Lemaître cosmologies. At the time static models for the universe were equally plausible from the observational viewpoint and it was not until 1929 when the observations by Edwin Hubble suggested for the first time that the universe is expanding.

The Big Bang

The observations show that the universe is expanding. Thus it was smaller in the past. Going far enough into the past, matter clumps together and as the density rises so does the temperature. Thus the universe was not only smaller in the past, it was also hotter. The young, hot and dense universe was also expanding rapidly, much faster than now when it is old, quite empty and cold. This is the basic picture of the hot big bang universe: when it was young, it was hot and expanding rapidly [8].

This simple picture is corroborated by almost equally simple observations. First, the universe is observed to be expanding. Second, if the universe really was hot in the past some residual radiation should be left. It is exactly what the CMB radiation is. The third piece of evidence is somewhat more subtle compared with the previous two. When the universe is hot enough there are no nuclei, since there are plenty[2] of high-energy photons to break them apart as soon as they from. As the universe cools down, eventually we reach the point when the photons no longer have high enough energies and nuclei begin to form. This is a well understood process since the energy scale in question, around MeV [15], is accessible in the laboratory, making it possible to study the physical processes in question in great detail. Thus it is possible to calculate the abundances of the light elements produced during this period called the nucleosynthesis and the calculations match the observed abundances [15, 17].

On the basis of those three observations, there really is no serious, or even less serious, contender to the hot big bang model for the big picture of the universe. That said, there are more than enough details to be ironed out.

[2]The baryon-to-photon ratio, $\eta_{10} = 10^{10}(n_b/n_\gamma)$, at the time is $\eta_{10} = 6.0 \pm 0.4$ [15] or $\eta_{10} = 6.225 \pm 0.170$ [16] as inferred from the light element abundances or from the WMAP data, respectively.

2.1.1 The Robertson-Walker Metric

Our picture of the universe is then something which is spatially isotropic and homogeneous at very large scales and expanding in time. To be exact, we can foliate the spacetime into constant time hypersurfaces that are maximally symmetric. The general metric for such a spacetime can be written as [18]

$$ds^2 = g_{00}(\tau)d\tau^2 + f^2(\tau)d\sigma^2, \tag{2.1}$$

where $d\sigma^2$ is the metric on the maximally symmetric space and independent on τ. The functions $g_{00}(\tau)$ and $f(\tau)$ are arbitrary, except for the requirement that $g_{00}(\tau) < 0$ and $f^2(\tau) > 0$ to give the manifold a Lorentzian signature. The function $f(\tau)$ is called the scale factor and gives the expansion of the spatial part, the metric of which is

$$d\sigma^2 = g_{ij}(x)dx^i dx^j. \tag{2.2}$$

The coordinates, for which $g_{00}(\tau)$ is independent of x^i and there are no cross terms $d\tau dx^i$, are called comoving coordinates and an observer at constant x^i a comoving observer. It should be clear from the above that the universe will look homogeneous and isotropic only for comoving observers.

The metric (2.1) can be written in a more familiar form that is the most general metric describing an expanding spatially homogeneous and isotropic spacetime [19, 18]. It was first derived by H.W. Robertson and A.G. Walker and is therefore known as the Robertson-Walker metric:

$$ds^2 = -dt^2 + a^2(t)\left[\frac{dr^2}{1-\kappa r^2} + r^2 d\theta^2 + r^2\sin^2(\theta)d\varphi^2\right]. \tag{2.3}$$

The function $a(t)$ is the scale factor and κ describes the curvature of the space. It's easy to see that scalings $r \to \lambda r$, $a \to \lambda^{-1}a$ and $\kappa \to \lambda^{-2}\kappa$ leave the metric unchanged, as they should, since they only correspond to a definition of the unit of length. There are different conventions in the normalisation of the scale factor and the curvature scale. One is to normalise κ to take the discrete values of ± 1 or 0 in which case the curvature scale and the scale factor are conventionally denoted by k and $R(t)$, respectively. Here we use the normalisation where the scale factor is unity today, $a(t_0) = a_0 = 1$ and the curvature scale can take any value.

In the case $\kappa = 0$ the spatial metric reduces back to the simple flat Euclidean space and is simply called the flat space. The cases $\kappa < 0$ and $\kappa > 0$ are called open and closed, respectively. The flat case is the most relevant since it is observationally favoured [20].

Conformal Time

The form of the metric in equation (2.3) corresponds to choosing $g_{00}(\tau)d\tau^2 = -dt^2$, where t is called the coordinate time. The only constraint in choosing the time coordinate is that we keep the Lorentzian signature and that we don't introduce any cross terms. Physically this means that the geometry must not depend on our definition of the unit of time.

One often used time coordinate is the conformal time η which is defined by

$$d\eta = \frac{dt}{a(t)}. \tag{2.4}$$

With this definition the scale factor becomes an overall factor in the metric (2.3):

$$ds^2 = a^2(\eta)[-d\eta^2 + \tilde{g}_{ij}dx^i dx^j]. \tag{2.5}$$

Conformal time is especially convenient when considering the flat case, since now the metric is conformally Minkowskian:

$$ds^2 = a^2(\eta)\eta_{\mu\nu}dx^\mu dx^\nu, \tag{2.6}$$

where $\eta_{\mu\nu} = \mathrm{diag}(-1, 1, 1, 1)$.

2.1.2 The Energy Components

The RW-metric (2.3) is obtained by geometrical consideration only and there is no need for a theory of gravity. Thus we only know what the universe looks like but not how it behaves. That is encoded in the time evolution of the scale factor, which is what we must find out. The theory of gravity we work in is the standard general relativity[3].

The Einstein field equation reads

$$R_{\mu\nu} - \frac{1}{2}Rg_{\mu\nu} = 8\pi G T_{\mu\nu}, \tag{2.7}$$

where the left side is defined by the metric. To complete the equations one needs to specify the energy-momentum tensor $T_{\mu\nu}$. We take the universe to be filled with ideal fluid, in which case $T_{\mu\nu}$ takes the following form

$$T_{\mu\nu} = (\rho + p)u_\mu u_\nu + p g_{\mu\nu}, \tag{2.8}$$

where u^μ is the four-velocity, ρ the energy density and p the pressure of the fluid. For the comoving observer u^μ must be of the form $u^\mu = (u^0, 0, 0, 0)$ for otherwise there would exist a preferred direction which would break the required isotropy. The four velocity satisfies the relation $u_\mu u^\mu = -1$, from which it follows that $u^0 = 1$. Thus the energy-momentum tensor in the fluid rest frame is

$$T_{\mu\nu} = \begin{bmatrix} \rho & 0 \\ 0 & p g_{ij} \end{bmatrix} \qquad \Rightarrow \qquad T^\nu_\mu = \mathrm{diag}(-\rho, p, p, p). \tag{2.9}$$

Before introducing the Einstein equations we'll see how the energy densities evolve in expanding space, which we'll find out from the energy conservation equation

$$T^\mu_{\nu;\mu} = 0. \tag{2.10}$$

The 0-component of which reads

$$\begin{aligned} T^\mu_{0;\mu} &= T^\mu_{0,\mu} + \Gamma^\mu_{\mu\lambda}T^\lambda_0 - \Gamma^\lambda_{\mu 0}T^\mu_\lambda \\ &= -\partial_t\rho - 3\frac{\dot{a}}{a}(\rho + p) = 0. \end{aligned} \tag{2.11}$$

[3]There are various extensions to the standard theory, but details of those are outside the scope of this thesis.

In order to write this equation down for the energy density only, we define the equation of state parameter w that relates ρ and p as

$$p = w\rho. \tag{2.12}$$

As such this appears to be of little use as we can always define such an quantity, no matter how complicated ρ and p are. However, in cosmology we are fortunate since for the fluids relevant to us, the equation of state parameter has a constant value independent of time. Thus we can write the equation (2.11) as

$$\frac{\dot{\rho}}{\rho} = -3(1+w)\frac{\dot{a}}{a}. \tag{2.13}$$

Integrating this gives us the behaviour of the energy density in terms of the scale factor

$$\rho \propto a^{-3(1+w)}. \tag{2.14}$$

Matter

The cosmologically relevant types of fluid are matter, radiation and vacuum energy. The matter, or dust, component refers to any nonrelativistic species of particles that have no pressure. The equation of state parameter for the matter component is thus zero, $w = 0$, meaning that their energy density behaves as

$$\rho \propto a^{-3}. \tag{2.15}$$

This is easily interpreted as the decrease in the number density as the volume of space expands while the number of particles remains constant. For nonrelativistic species the energy density is dominated by the rest mass which in turn is proportional to the number density.

Radiation

Radiation, which refers to any highly relativistic particle species or actual electromagnetic radiation, has a pressure which is one third of the energy density. Thus $w = \frac{1}{3}$ which givers

$$\rho \propto a^{-4}. \tag{2.16}$$

Here we also have the decrease in the number density which gives a^{-3} and the additional a^{-1} term comes from the redshifting of the energy due to the expansion of space.

Vacuum energy

The last component is the vacuum energy or cosmological constant which has the curious property of negative presssue with equation of state $w = -1$. This means that its energy density remains constant

$$\rho \propto a^{0} = 1. \tag{2.17}$$

The equation of state can be seen from the Einstein equation. The symmetries of the equations do not change if one adds a constant, Λ, to the equations

$$R_{\mu\nu} - \frac{1}{2}Rg_{\mu\nu} + \Lambda g_{\mu\nu} = 8\pi G T_{\mu\nu}. \tag{2.18}$$

Of course one can write the constant term to the right side and think of it as included in the $T_{\mu\nu}$. Now take this constant term to be the only component of $T_{\mu\nu}$, i.e., $T_{\mu\nu} = bg_{\mu\nu}$, where b is a constant. Comparing this to the energy-momentum tensor of the ideal fluid, $T_{\mu\nu} = (\rho + p)u_\mu u_\nu + pg_{\mu\nu}$, we see that the cosmological constant is described by an ideal fluid with $b = p = -\rho$. Of course, in this case there is no dependence on the four-velocity nor is there any evolution, it is somewhat questionable to talk about a fluid.

2.1.3 The Friedmann Equations

The Einstein equations (2.7) give two separate equations, the 0-0–component and i-j–component; the latter are all equal due to the spatial isotropy. These equations can be written as

$$\left(\frac{\dot{a}}{a}\right)^2 = \frac{8\pi G}{3}\rho - \frac{\kappa}{a^2}, \tag{2.19}$$

$$\frac{\ddot{a}}{a} = -\frac{4\pi G}{3}(\rho + 3p). \tag{2.20}$$

In the standard nomenclature the equation (2.19) is called the Friedmann equation and the equation (2.20) the second Friedmann equation. These and the energy continuity equation (2.13) are not independent of each other, but one can for example obtain (2.20) from (2.19) and (2.13).

The Hubble parameter, which gives the rate of expansion, is defined as

$$H \equiv \frac{\dot{a}}{a}. \tag{2.21}$$

The Hubble constant refers to its current value $H(t_0)$ and is denoted by H_0. The observed value is $H_0 = 70.1 \pm 1.3\,\mathrm{km\,s^{-1}Mpc^{-1}}$ [13]. It is common to define the shorthand notation h as

$$H = 100h\,\mathrm{km\,s^{-1}Mpc^{-1}}. \tag{2.22}$$

The reciprocal of H_0 has a dimension of distance or time and is called the Hubble distance or Hubble time and it is the common factor in all distance scales

$$H_0^{-1} = 3000\,h^{-1}\mathrm{Mpc} \tag{2.23}$$

$$= 9.78 \times 10^9\,h^{-1}\mathrm{yr}. \tag{2.24}$$

The critical density ρ_c is the density at which the curvature term vanishes in the Friedmann equation (2.19):

$$\rho_c = \frac{3H^2}{8\pi G} = 3H^2 M_{\mathrm{Pl}}^2. \tag{2.25}$$

The density parameter is the energy density given as fraction of the critical density

$$\Omega_i = \frac{\rho_i}{\rho_c}, \tag{2.26}$$

where i denotes the type of energy with m for matter, c for CDM, r for radiation and Λ for vacuum energy. With these we can now write the Friedmann equation in the following form

$$\Omega_{\mathrm{tot}} - 1 = \frac{\kappa}{(aH)^2}. \tag{2.27}$$

2.1.4 Evolution of the Scale Factor and the Horizon

The particle horizon is the distance light has travelled since the big bang and thus gives the scale at which causal processes can happen. Considering radial motion the RW-metric (2.3) gives

$$\int_0^r \frac{dr}{\sqrt{1-\kappa r^2}} = \int_0^t \frac{dt}{a(t)}. \tag{2.28}$$

The left-hand side gives the comoving coordinate distance, d_c, and can be integrated for all geometries

$$d_c = \begin{cases} |\kappa|^{-\frac{1}{2}} \arcsin(|\kappa| r) & \text{when } \kappa > 0 \\ r & \text{when } \kappa = 0 \\ |\kappa|^{-\frac{1}{2}} \operatorname{arsinh}(|\kappa| r) & \text{when } \kappa < 0 \end{cases} \tag{2.29}$$

$$\equiv \operatorname{sinn}_\kappa^{-1}(r) \tag{2.30}$$

The right-hand side, however, does not integrate that easily. The evolution of the scale factor is given by the Friedmann equation as stated above and gives

$$\int_0^{a(t_0)=1} \frac{da}{a(t)} = \frac{1}{H_0} \int_0^{a(t_0)=1} \frac{da}{\sqrt{\Omega_{\mathrm{m}_0} a + (1-\Omega_{\mathrm{tot}}) a^2 + \Omega_{\mathrm{r}_0} a^3 + \Omega_{\Lambda_0} a^4}}. \tag{2.31}$$

This does not integrate to elementary functions so to use the full equation one would need to evaluate it numerically.

However, it is not necessary to use the whole equation. We know the universe to be nearly flat, so we can ignore the curvature part. Considering only one kind of energy at the time we get the behaviour for the scale factor when that type of energy dominates the energy density of the universe:

$$a(t) = \begin{cases} \left(\frac{t}{t_0}\right)^{\frac{1}{2}} & \text{for radiation: } \rho \propto a^{-4}, \\ \left(\frac{t}{t_0}\right)^{\frac{2}{3}} & \text{for matter: } \rho \propto a^{-3}. \end{cases} \tag{2.32}$$

From this we get the horizons for the radiation and matter dominated (RD / MD) cases

$$d(t) = a(t) d_c = a(t) \int_0^t \frac{dt'}{a(t')} = \begin{cases} 2t & \text{(RD)} \\ 3t & \text{(MD).} \end{cases} \tag{2.33}$$

In both cases the scale factor behaves like $a \propto t^n$, in which case the Hubble parameter is

$$H = nt^{-1}. \tag{2.34}$$

Thus the horizon can be written as

$$d(t) = \begin{cases} 2t = H^{-1} & \text{(RD)} \\ 3t = 2H^{-1} & \text{(MD).} \end{cases} \tag{2.35}$$

It is common to use the terms Hubble length and horizon interchangeably while they are not exactly the same thing.

The cosmological redshift[4] is defined as

$$a = \frac{1}{1+z}. \tag{2.36}$$

One measure of distance that is relevant when discussing CMB observations is the angular diameter distance $d_A(z)$. This gives the distance to an object at redshift z that subtends an angle θ on the sky and has a proper diameter s. The RW-metric along the coordinate θ gives

$$ds = a(t)\, r\, d\theta \quad \Rightarrow \quad s = a(t)\, r\, \theta. \tag{2.37}$$

From standard geometry we know

$$\theta = \frac{s}{d_A} \quad \Rightarrow \quad d_A(t) = \frac{s}{\theta} = a(t)r. \tag{2.38}$$

Now the expression for the angular diameter distance to an object at redshift z in the flat universe is

$$d_A(z) = \frac{H_0^{-1}}{1+z} \int_{\frac{1}{1+z}}^{1} \frac{da}{\sqrt{\Omega_{\mathrm{m}_0} a + \Omega_{\mathrm{r}_0} a^3 + \Omega_{\Lambda_0} a^4}}. \tag{2.39}$$

2.1.5 Brief Thermal History of the Universe

Here we briefly overview the thermal history of the universe and point out the most relevant events that took place since the big bang. A more detailed discussion can, for example, be found in [8].

The furthest era we can practically think of is the Planck scale at $t \sim 10^{-43}$ s and $T \sim 10^{19}$ GeV. Beyond this, the quantum effects of gravity become important and the quantum theory of gravity that would describe our universe is still a work in progress.

When the temperature has come down to around 100 GeV at 10^{-10} s we have the electroweak phase transition when the electromagnetism and the weak interaction separate from one another. After this, at ∼100 MeV and 10^{-4} s the quarks condense to form hadrons and by 10 MeV we have only photons, neutrinos, electrons, positrons, neutrons and protons left in a thermal equilibrium.

[4] The cosmological redshift is due to the expansion of space. Objects, such as galaxies can and do have redshift due to their intrinsic motion in space but on large scales this component is much smaller compared to the cosmological one. On small enough distances this does not necessarily hold. A well-known example of this it the Andromeda galaxy, which we actually see as blueshifted since it is moving towards us.

The neutrinos decouple from the other species of particles at 1 s when the temperature is 1 MeV. Soon after the temperature drops below the electron rest mass and the electrons and positrons annihilate one another. Some electrons are left due to the asymmetry that there is more matter than antimatter present [8].

The nucleosynthesis, when the until then freely floating protons and neutrons bind together into atomic nuclei takes place at around $T \sim$0.1 MeV or $t \sim$100 s. At that point the temperature has come down enough that the photons no longer break apart the newly formed nuclei. After this, when the temperature reaches 1 eV we have the matter-radiation–equality at $t_{eq} \sim 10^4$ years when the energy density of the radiation has reached that of the matter component. After this the matter component dominates the evolution of the universe.

From the point of view of the CMB physics, the most interesting event takes place at 380000 year old universe [13] when the temperature has come down to 0.3 eV. At this point the electrons and nuclei combine to form neutral atoms in a process that is called the recombination. Now that the photons do not scatter from the free charges around, the mean free path of a photon grows larger than the size of the horizon. These photons then constitute the CMB sky we observe today. The recombination happens this late, instead of at the hydrogen binding energy of 13.6 eV because of the great number of photons. There are $\sim 10^{10}$ photons for each electron [16] meaning that there are enough high-energy photons around to break up the atoms even if the temperature is below 13.6 eV.

After this the first structures are born that eventually grow up to form all the structure we see around ourselves. When the first stars are born, which takes a few hundred million years [13], the radiation from them reionises the universe. However, at this point the matter in the universe is already quite dilute, so that only a fraction of the photons rescatter. Should the supernova observations be correct and there really is a dark energy component, it has recently overtaken the matter part and now we live in a dark energy dominated universe.

2.2 Inflation

The paradigm of inflation was originally suggested around 1980s [21, 22, 23] to explain a set of problems troubling the standard big bang scenario that we will discuss below. Since then there has been a number of different models of inflation, but they all share the same basic idea. The assumption is that when the universe was a fraction of a second old, the vacuum energy dominated over all other energy forms for some time, during which the scale factor grows at least quasiexponentially.

Perhaps the greatest outcome from inflation after all is not related to the reasons it was originally conceived, but the fact that it provides a mechanism to generate the small deviations from the homogeneity [24]. These small inhomogeneities then grow over time to form the currently observed large scale structure. A rather nice feature from an idea deviced to explain the homogeneity in the first place.

2.2.1 Problems of the Standard Big Band

Even with the success of the standard big bang scenario it is not without its share of problems. These are not issues that are incorrect *per se*, but rather something for which we do not get a satisfactory answer within the standard scenario.

Horizons

The microwave background is formed at photon recombination at $z \sim 1100$ while the matter-radiation equality is at $z \sim 3200$ [13]. Thus the universe is already well matter dominated when the CMB is formed. Ignoring the brief period of radiation domination, we assume the universe to evolve as matter dominated. The size of comoving horizon at photon decoupling d_{c*} compared to the current horizon d_{c0} is

$$\frac{d_{c*}}{d_{c0}} = 1100\frac{t_*}{t_0} \approx 10^{-2} \tag{2.40}$$

for $t_* = 4 \cdot 10^5$ yr and $t_0 = 1.4 \cdot 10^{10}$ yr [13].

Thus we find out that the last scattering surface has formed from $\sim 10^4$ regions that were not causally connected at the time. The ratio of the horizons converts to a angle of $\sim 1^\circ$ in the last scattering surface meaning that observations on scales larger than this observe causally unconnected regions.

The difference between the horizons only grows larger if we consider an earlier time, such as nucleosynthesis that took place when the universe was about a second old. However, based on observations, the nucleosynthesis seems to have produced the same amount of nuclei on all these causally unconnected regions.

Flatness

Considering our normal types of energy densities the scale factor evolves as $a \propto t^n$, with $n \in]0, 1[$. Thus the Hubble parameter grows as $H \propto t^{-1}$. Since H^{-1} is the physical horizon length $(aH)^{-1}$ is the comoving horizon. So we have $(aH)^{-1} \propto t^{1-n}$ with $1 - n > 0$. This just means that the comoving horizon grows in time for a universe that contains normal matter or radiation. The Friedmann equation (2.27) now reads

$$|\Omega - 1| \propto \frac{1}{a^2H^2} \propto t^{2(1-n)} = t^m, \quad m > 0. \tag{2.41}$$

As the universe today appears to be quite flat, according to above relation the deviation from exact flatness must have been even smaller in the past. If $|\Omega - 1| \simeq 1$ today, then around the time of nucleosynthesis $|\Omega - 1| \leq 10^{-17}$ and at Planck scale of $t_{\mathrm{Pl}} = 10^{-43}$ s we get $|\Omega - 1| \leq 10^{-60}$.

Relic Particles

In the supersymmetric theories of the particle physics there is a selection of heavy stable particles. If the temperature has been high enough in the early universe, like in the standard scenario it should

have been, then the heavy particles produced at the high temperature should still be present. Then their abundances can easily exceed the critical density making $\Omega_{\rm tot} > 1$ [24]. However, no such relics are observed to exist.

2.2.2 Accelerated Expansion

In the broadest sense the inflation is a period during which the expansion of the universe is accelerating:

$$\ddot{a} > 0 \quad \Rightarrow \quad \frac{d}{dt}\frac{1}{aH} < 0. \tag{2.42}$$

The latter form tells us that during the inflationary period the comoving horizon is decreasing with time, meaning that the observable universe is actually becoming smaller.

Now it is easy to see why inflation solves the abovementioned problems. From the latter form of (2.42) we see that during inflation the universe is driven towards flatness rather than away from it. Since the comoving horizon is shrinking, an isotropic and homogeneous patch of space, smaller than the comoving horizon before inflation, can now be larger than the comoving horizon after the inflation. The unwanted heavy relic particles are simply diluted away as the universe expands, as long as they are produced before the inflationary period.

Now the only requirement for inflation is that it lasts long enough. The amount of inflation is conventionally given as the factor by which the scale factor grows during the inflationary period, the e-folds:

$$N \equiv \ln \frac{a_{\rm end}}{a_{\rm init}}. \tag{2.43}$$

In order for the discussed problems to be taken care of, roughly 60 e-folds of inflation are required [25]

The next question is how the period of inflation can be realised? From the condition for inflation (2.42) and the second Friedmann equation (2.20) we see that the inflation takes place when the universe is filled with energy that satisfies the condition

$$\rho + 3p < 0. \tag{2.44}$$

From this it is evident that the garden variety cosmological constant suits just fine to produce inflation. Unfortunately, cosmological constant being true to its name, that is, being constant and remaining so while all other forms of energy with $\rho \propto a^{-n}$, $n > 0$, tend to zero density. Thus we would be left with a flat and cold universe filled with nothing but the vacuum energy, something that quite contradicts our observations. Obviously, a better explanation is called for.

2.2.3 Scalar Fields

Instead of just an *ad hoc* cosmological constant we consider a homogeneous scalar field[5] called the inflaton with Langrangian

$$\mathcal{L} = \frac{1}{2}\partial_\mu\varphi\partial^\mu\varphi - V(\varphi) = \frac{1}{2}\dot{\varphi}^2 - V(\varphi), \tag{2.45}$$

where the gradient term is absent since the field is homogeneous, i.e., $\varphi = \varphi(t)$. This Lagrangian gives the equation of motion for the field

$$\ddot{\varphi} + 3H\dot{\varphi} + V_{,\varphi}(\varphi) = 0, \tag{2.46}$$

where $V_{,\varphi}(\varphi)$ denotes a derivative with respect to φ. The equation (2.46) is a oscillator equation with a damping term coming from the expansion of space. The generalisation to many fields is simple and we get the same equation for each field

$$\ddot{\varphi}_I + 3H\dot{\varphi}_I + V_{,\varphi_I}(\varphi) = 0. \tag{2.47}$$

Even if there is no explicit interaction between the fields, i.e. $V(\varphi) = \sum V(\varphi_I)$, they still do couple through gravity via the evolution of H, which is governed by all of the fields. However, we only consider a single field here, as the inclusion of multiple fields does not bring anything relevant when discussing the background evolution only. When perturbations are included in the next chapter, the situation changes dramatically and there is a fundamental difference between one- and multi-field cases.

The energy-momentum tensor for the scalar field reads

$$T_{\mu\nu} = \partial_\mu\varphi\partial_\nu\varphi + \mathcal{L}g_{\mu\nu}. \tag{2.48}$$

Comparing this to the energy-momentum tensor of the ideal fluid (2.8) we obtain

$$\rho = \frac{1}{2}\dot{\varphi}^2 + V(\varphi), \tag{2.49}$$

$$p = \frac{1}{2}\dot{\varphi}^2 - V(\varphi). \tag{2.50}$$

If we then consider a field that moves slowly enough, such that $\frac{1}{2}\dot{\varphi}^2 \ll V(\varphi)$, we see that the field closely mimics the cosmological constant as $p \sim -\rho$ giving rise to a quasiexponential growth of the scale factor.

The overall picture is that the universe inflates while the field rolls down the potential slowly enough for the above condition to hold, meaning that the potential needs to be flat enough. The inflationary phase ends when this condition breaks, usually as the inflaton reaches the bottom of the potential. Now, the exponential expansion has lead the universe to be completely empty and cold with all the particles that existed before simply diluted away as $\rho \propto e^{-nHt}$, $n > 0$. All the energy density is stored in the inflaton field which then must decay into the standard model particles and reheat the universe so that the normal hot big bang era ensues.

[5] In many sense an equally *ad hoc* construct, although the hope is that it would be easier to come up with such a field than a plain cosmological constant from some fundamental theory. However, this is still very much an open question.

Slow-Roll

In addition to the requirement that $\frac{1}{2}\dot{\varphi}^2 \ll V(\varphi)$ we also demand that $\ddot{\varphi} \ll \dot{\varphi}$. Now the equation of motion and the Friedmann equation read

$$H^2 \simeq \frac{1}{3M_{\rm Pl}^2} V, \tag{2.51}$$

$$3H\dot{\varphi} \simeq -V_{,\varphi}, \tag{2.52}$$

The above approximation is valid when these two conditions hold

$$\epsilon \equiv \frac{M_{\rm Pl}^2}{2}\left(\frac{V'}{V}\right)^2 \ll 1, \tag{2.53}$$

$$\eta \equiv M_{\rm Pl}\left(\frac{V''}{V}\right), \quad |\eta| \ll 1, \tag{2.54}$$

where we defined the slow-roll parameters ϵ and η. These are necessary but not sufficient conditions as they only constrain the form of potential and one can choose $\dot{\varphi}$ to break the slow-roll approximation. For the simplest model of inflation with quadratic potential $V(\varphi) = \frac{1}{2}m^2\varphi^2$ the inflation takes place when $\varphi^2 > 2M_{\rm Pl}^2$.

The amount of inflation produced by the slow-rolling scalar field is

$$N = \ln\frac{a_{\rm end}}{a_{\rm init}} = \int_{t_{\rm init}}^{t_{\rm end}} dtH = \frac{1}{M_{\rm Pl}^2}\int_{\varphi_{\rm end}}^{\varphi_{\rm init}} d\varphi \frac{V}{V'}. \tag{2.55}$$

In order to produce the desired 60 e-folds of inflation when $V(\varphi) = \frac{1}{2}m^2\varphi^2$ the initial value for the field must be $\varphi \approx 16\, M_{\rm Pl}$. Since in this case the number of e-folds goes as φ^2, for example, if $\varphi = 100\, M_{\rm Pl}$ we get $N \approx 2500$. Thus it is simple to have the inflation last long enough, provided that the field initially has a large enough value.

Chapter 3

Perturbations and the Cosmic Microwave Background

Thus far we have taken the universe to be spatially homogeneous, isotropic and expanding in time. On small scales it is obvious that this is not the case and looking at the galaxy distributions we see structure on the larger scales as well. Fortunately, the deviations from the perfect FLRW-cosmology, on cosmologically relevant scales, are small enough so we can work close to FLRW-model. From here on we will only consider the flat universe as that is supported by the observations.

It is not our purpose to give a detailed presentation of the cosmological perturbation theory, but instead to present an overview how we get from small perturbations in the early universe to the observed CMB anisotropies in the sky. For the full details we refer to the standard works on perturbation theory [26, 27]

3.1 Perturbations in the Background

We work close to the simple FLRW-model which is referred to as the background, the evolution of which was discussed in the previous chapter. Then we introduce a small deviation from this and write the Einstein equation to first order in this perturbation.

We are thus considering two spacetimes, the simple isotropic and homogeneous background that is a function of time only, and the real perturbed one. The metric for our perturbed spacetime can be written as

$$g_{\mu\nu} = \bar{g}_{\mu\nu} + \delta g_{\mu\nu}, \tag{3.1}$$

where $\bar{g}_{\mu\nu}$ is the background RW-metric and $\delta g_{\mu\nu}$ is small deviation from it. We will take the first and second derivatives of the perturbation to be small as well.

From the metric we can calculate the Einstein tensor which also can be split into a background

and a perturbation part. The same can be done for the energy-momentum tensor as well:

$$G_{\mu\nu} = \bar{G}_{\mu\nu} + \delta G_{\mu\nu}, \tag{3.2}$$

$$T_{\mu\nu} = \bar{T}_{\mu\nu} + \delta T_{\mu\nu}. \tag{3.3}$$

The Einstein equation is then of course

$$G_{\mu\nu} = 8\pi T_{\mu\nu} \quad \Rightarrow \quad \bar{G}_{\mu\nu} + \delta G_{\mu\nu} = 8\pi(\bar{T}_{\mu\nu} + \delta T_{\mu\nu}). \tag{3.4}$$

But since the background is just the simple FLRW-universe we know that part already satisfies the Einstein equations, i.e., $\bar{G}_{\mu\nu} = 8\pi\bar{T}_{\mu\nu}$ and thus we are left with the equations for the perturbation part only

$$\delta G_{\mu\nu} = 8\pi\delta T_{\mu\nu}. \tag{3.5}$$

3.1.1 The Perturbed Metric

Now it is more convenient to work with the conformal time η since then our flat background metric is simply

$$ds^2 = \bar{g}_{\mu\nu}dx^\mu dx^\nu = a^2(\eta)[-d\eta^2 + \delta_{ij}dx^i dx^j] = a^2(\eta)\eta_{\mu\nu}. \tag{3.6}$$

Now the perturbed metric can be written as

$$g_{\mu\nu} = \bar{g}_{\mu\nu} + \delta g_{\mu\nu} = a^2(\eta)[\eta_{\mu\nu} + h_{\mu\nu}], \tag{3.7}$$

where $h_{\mu\nu}$ and its first and second derivatives are taken to be small. Since we are calculating everything at first order it means that all terms that are $\mathcal{O}(h^2)$ and higher are dropped. Thus the inverse metric is

$$g^{\mu\nu} = a^{-2}(\eta)[\eta^{\mu\nu} - h^{\mu\nu}]. \tag{3.8}$$

Now, define the parts of $h_{\mu\nu}$ as

$$[h_{\mu\nu}] = \begin{bmatrix} -2A & -B_i \\ -B_i & -2D\delta_{ij} + 2E_{ij} \end{bmatrix}, \tag{3.9}$$

where the trace of the spatial part is in D, i.e., $D = -\frac{1}{6}h^i_i$ and E_{ij} is traceless, $\delta^{ij}E_{ij} = 0$. Thus the general line element of the perturbed spacetime is

$$ds^2 = a^2(\eta)\{-(1+2A)d\eta^2 - 2B_i d\eta dx^i + [(1-2D)\delta_{ij} + 2E_{ij}]dx^i dx^j\}. \tag{3.10}$$

The background is a function of time only and its evolution is encoded in the scale factor, $a = a(\eta)$. The perturbed part, on the other hand, can and does depend on the coordinates, i.e., $h_{\mu\nu} = h_{\mu\nu}(\eta, x^i)$.

3.1.2 Gauge and Gauge Transformations

As discussed above, we are dealing with two spacetimes, the background one and the perturbed one. The correspondence between these two is by no means unique. Given a perturbed spacetime, describing the real, slightly inhomogeneous universe, there are an infinite number of ways to choose which point in that spacetime corresponds to which point in the background spacetime. This choice of the correspondence, i.e., the choice of $[h_{\mu\nu}]$, is the gauge.

However, there is no one true gauge to rule them all. Some gauges are more appropriate in some situation than others and often it is simply a matter of personal preference. In this work we will employ the so called conformal-Newtonian gauge, which we will define shortly, that is appropriate for our purposes.

What we are interested in are the various perturbed quantities, such as the energy density. In general, we can have scalar, vector or tensor fields

$$\begin{aligned} s &= \bar{s} + \delta s \\ w^\mu &= \bar{w}^\mu + \delta w^\mu \\ A^\nu_\mu &= \bar{A}^\nu_\mu + \delta A^\nu_\mu. \end{aligned} \tag{3.11}$$

Since we know the background to be highly symmetric, the background parts of the above quantities must honour this requirement, thus

$$\bar{w}^\mu = (\bar{w}^0, 0) \quad \text{and} \quad \bar{A}^\nu_\mu = \begin{bmatrix} \bar{A}^0_0 & 0 \\ 0 & -\frac{1}{3}\delta^j_i \bar{A}^k_k \end{bmatrix} \tag{3.12}$$

where these are only dependent on time.

When dealing with the perturbed quantities we have the gauge freedom and the question is how these quantities change if we change the gauge. To go from one gauge to the other, we make the coordinate transformation

$$\tilde{x}^\mu = x^\mu + \xi^\mu, \tag{3.13}$$

where ξ^μ and its derivative are first order small. Under this kind of transformation we get the following transformations

$$\widetilde{\delta s} = \delta s - \bar{s}'\xi^0 \qquad \begin{aligned} \widetilde{\delta w}^0 &= \delta w^0 + \xi^0_{,0}\bar{w}^0 - \bar{w}^0_{,0}\xi^0 \\ \widetilde{\delta w}^i &= \delta w^i + \xi^i_{,0}\bar{w}^0 \end{aligned} \qquad \begin{aligned} \widetilde{\delta A}^0_0 &= \delta A^0_0 - \bar{A}^0_{0,0}\xi^0 \\ \widetilde{\delta A}^0_i &= \delta A^0_i + \frac{1}{3}\xi^0_{,i}\bar{A}^k_k - \xi^0_{,0}\bar{A}^0_0 \\ \widetilde{\delta A}^i_0 &= \delta A^i_0 + \xi^i_{,0}\bar{A}^0_0 - \frac{1}{3}\xi^i_{,0}\bar{A}^k_k \\ \widetilde{\delta A}^j_i &= \delta A^j_i - \frac{1}{3}\delta^j_i \bar{A}^k_{k,0}\xi^0. \end{aligned} \tag{3.14}$$

3.1.3 Scalar, Vector and Tensor Separation

In addition to the gauge transformations that change the correspondence between the background and the perturbed spacetime we can consider transformations of the background while keeping the

gauge fixed. Like stated many times over, our background is isotropic and homogeneous and we do not want to change this. This choice of background means that we have uniquely fixed our constant time hypersurfaces which leave us with two kind of transformations.

One is the simple reparametrisation of the time coordinate as defining the unit of time obviously can't affect the background geometry. Since we have already chosen to use the conformal time, this type of transformation is not relevant to us now.

The second kind are the transformations of the spatial part of the background. Since the time part was already taken care of, these transformations must be independent of time. Also, as the spatial part of our background is already conveniently the Euclidian one we don't want to change this either because a more complicated coordinate system would serve no purpose. Thus we are left with the 3-dimensional rotations. The full transformation is then

$$x^{\mu'} = X^{\mu'}_{\nu} x^{\nu}, \quad \text{with} \quad X^{\mu'}_{\nu} = \begin{bmatrix} 1 & 0 \\ 0 & R^{j'}_{i} \end{bmatrix}, \tag{3.15}$$

where $R^{j'}_{i}$ is the rotation matrix.

Now, transforming our metric with this matrix reveals the reason for choosing the components of the perturbation $[h_{\mu\nu}]$ as we did:

$$\begin{aligned} A' &= A & B_{i'} &= R^{j}_{i'} B_j \\ D' &= D & E_{i'j'} &= R^{k}_{i'} R^{l}_{j'} E_{kl}. \end{aligned} \tag{3.16}$$

So the different parts behave like scalars, a vector and a tensor under the rotations.

This result can still be refined a bit further. In Euclidean space we can decompose a vector into two parts and a tensor into three. For the vector these parts are

$$B_i = -B_{,i} + B^{\mathrm{v}}_i, \tag{3.17}$$

where B is a scalar function and B^{v}_i a divergenceless vector field, $\delta^{ij} B^{\mathrm{v}}_{i,j} = 0$. Similarly for the tensor field we have a scalar E^{s}_{ij}, vector E^{v}_{ij} and tensor E^{t}_{ij} parts

$$E_{ij} = E^{\mathrm{s}}_{ij} + E^{\mathrm{v}}_{ij} + E^{\mathrm{t}}_{ij}, \tag{3.18}$$

where the components are a bit more complicated than in the vector decomposition

$$\begin{aligned} E^{\mathrm{s}}_{ij} &= E_{,ij} - \frac{1}{3}\delta_{ij}\delta^{kl} E_{,kl} \\ E^{\mathrm{v}}_{ij} &= -\frac{1}{2}(E_{i,j} + E_{j,i}) \quad \text{with} \quad \delta^{ij} E_{i,j} = 0 \\ E^{\mathrm{t}}_{ij} &\quad \text{with} \quad \delta^{ik} E^{\mathrm{t}}_{ij,k} = 0 \quad \text{and} \quad \delta^{ij} E^{\mathrm{t}}_{ij} = 0, \end{aligned} \tag{3.19}$$

where E is a scalar function, E_i a divergenceless vector and E_{ij} a tensor. Each of the parts is separately made traceless. Additionally, the vector part is constructed as symmetric while the tensor part is assumed to be so. Finally the conditions on the tensor part make it also transverse[1].

[1]The Fourier components, $E^{\mathrm{t}}_{ij}(\vec{k})$, of E^{t}_{ij} have non-zero components only perpendicular to the direction of the Fourier mode. For example if $k \parallel \hat{z}$, $E^{\mathrm{t}}_{ij}(\vec{k}) = 0$ for $i, j = 3$.

Now under the transformation (3.15) these components transform as

$$\begin{aligned} A' &= A \qquad B' = B \qquad D' = D \qquad E' = E \\ B^{\mathrm{v}}_{i'} &= R^{j}_{i'} B^{\mathrm{v}}_{j} \qquad E_{i'} = R^{j}_{i'} E_{j} \\ E^{\mathrm{t}}_{i'j'} &= R^{k}_{i'} R^{l}_{j'} E^{\mathrm{t}}_{kl} \end{aligned} \tag{3.20}$$

Thus we have decomposed the perturbed metric into scalar, vector and tensor parts according to their transformation properties under the three-dimensional rotations of the form (3.15).

Since we are doing first order perturbation theory we can study the evolution of the scalar, vector and tensor parts separately. This is simply because A, D, B_i and E_{ij} are, by definition, first order small and thus all mixed terms, like AB_i, are second order small and we can discard such terms. The total perturbation is simply the sum of the scalar, vector and tensor parts.

The most relevant part, and the one we will concentrate on, is the scalar perturbation. This is because this part on the metric side couples to the energy density and pressure and thus describes the process that eventually leads to the formation of structure in the universe.

The vector part couples to the velocity perturbations, but this type of perturbation decays in the expanding universe and thus generally assumed unimportant. However, if there are some sources for the velocity perturbation in the early universe, like primordial magnetic fields, then the vector perturbations might survive [28]. We do not consider such a situation here and thus take the vector perturbation to be absent.

The tensor perturbations are simply gravitational waves. If strong enough, they will have important cosmological implications, but currently they still remain unobserved. Thus we will not study then in detail, but do mention them where relevant.

3.1.4 The Gauge Choice

From now on we will only consider the scalar perturbations in more detail as that is the cosmologically most relevant one. Thus we have 4 degrees of freedom in choosing the perturbed metric. This scalar part was defined by the properties of the perturbed metric under rotations of the background when keeping the gauge fixed. We still have the gauge freedom to use and this allows us to set any two of the scalar perturbations to zero. The conformal-Newtonian gauge refers to the gauge where we choose $B = 0$ and $E = 0$. The remaining perturbations quantities A and D are then commonly denoted as Φ and Ψ and called the Bardeen potentials. Thus our perturbed metric, when only considering the scalar perturbations, gets the following nice and simple form

$$ds^2 = a^2(\eta)[-(1+2\Phi)d\eta^2 + (1-2\Psi)\delta_{ij}dx^i dx^j]. \tag{3.21}$$

The function Ψ is sometimes also called the curvature perturbation, since the Ricci scalar on the hypersurface of constant time is

$$R^{(3)} = 4a^{-2}\nabla^2\Psi. \tag{3.22}$$

We will be using this gauge from now on. From this metric we can then calculate the left-hand side of the Einstein equation.

3.1.5 Perturbed Energy Tensor

In order to get the full set of Einstein equations we need the perturbed energy-momentum tensor as well. The process is similar to that above which gave us the perturbed metric. Our background energy tensor is that of the perfect fluid and now we introduce a small perturbation to that, i.e.,

$$T^{\nu}_{\mu} = \bar{T}^{\nu}_{\mu} + \delta T^{\nu}_{\mu}. \tag{3.23}$$

This perturbation can also be decomposed into scalar, vector and tensor parts that couple to the corresponding metric perturbations. Naturally, the choice of gauge has an effect for the energy tensor as well.

At the end of the day and few sheets of paper, the perturbed energy tensor for scalar perturbations in the conformal-Newtonian gauge is

$$T^{\nu}_{\mu} = \begin{bmatrix} -\bar{\rho} - \delta\rho & -(\bar{\rho} + \bar{p})v_{,i} \\ (\bar{\rho} + \bar{p})v_{,i} & (\bar{p} + \delta p)\delta^{j}_{i} + \bar{p}(\Pi_{,ij} - \frac{1}{3}\delta^{j}_{i}\delta^{kl}\Pi_{,kl}) \end{bmatrix}, \tag{3.24}$$

where v is the scalar part of the velocity perturbation and Π the scalar part of the tensor and describes the deviation from the perfect fluid.

3.1.6 Curvature Perturbation

We have fixed our gauge to be the conformal-Newtonian one. Therefore we can simply take the metric (3.21) to give the Einstein tensor and with the perturbed energy tensor (3.24) obtain the evolution equations for the perturbation quantities. However, this is not the only approach. One can obtain the evolution equations without specifying the gauge or use a gauge that does not completely fix the coordinates, such as the synchronous gauge [26]. In these cases there is some residual gauge freedom still left. In such a case, it is more convenient to define quantities that are invariant under gauge transformations instead of using the "plain" perturbed quantities such as A or E.

One commonly used such gauge invariant quantity is the comoving curvature perturbation $\mathcal{R}$ defined as:

$$\mathcal{R} \equiv \Psi + \frac{2}{3(1+w)}(\mathcal{H}^{-1}\Psi' + \Phi). \tag{3.25}$$

We refer to this parameter in our papers since $\mathcal{R}$ the quantity that is given as the initial value for the computer code calculating the CMB angular power spectra.

3.1.7 Entropy Perturbation

The entropy density s is given by $s = S/V$. It is dominated by the contribution from photons [8], i.e., $s \propto n_\gamma$, where n_γ is the number density of photons. Thus the entropy per particle of type i is $S/N_i = s/n_i \propto n_\gamma/n_i$. From this the entropy perturbation is then given by

$$\frac{\delta(n_\gamma/n_i)}{n_\gamma/n_i} = \frac{\delta n_\gamma}{n_\gamma} - \frac{\delta n_i}{n_i}. \tag{3.26}$$

Now, let us define the total entropy perturbation as

$$\mathcal{S}_{\rm tot} \equiv \mathcal{H}\left(\frac{\delta p}{p'} - \frac{\delta\rho}{\rho'}\right). \tag{3.27}$$

In the early universe we have matter (m) and radiation (r) meaning

$$\begin{aligned}
\delta p_{\rm tot} &= \delta p_{\rm r} + \delta p_{\rm m} = \delta p_{\rm r} = \tfrac{1}{3}\delta\rho_{\rm r} \\
\delta\rho_{\rm tot} &= \delta\rho_{\rm r} + \delta\rho_{\rm m} \\
p'_{\rm tot} &= p'_{\rm r} + p'_{\rm m} = \tfrac{1}{3}\rho'_{\rm r} = -\tfrac{4}{3}\mathcal{H}\rho_r \\
\rho'_{\rm tot} &= \rho'_{\rm r} + \rho'_{\rm m} = -4\mathcal{H}\rho_{\rm r} - 3\mathcal{H}\rho_{\rm m},
\end{aligned} \tag{3.28}$$

where the last two equations result from using the energy continuity equation written in conformal time:

$$\rho' = -3\mathcal{H}(1+w)\rho. \tag{3.29}$$

Thus the total entropy perturbation can be written as

$$\mathcal{S}_{\rm tot} = -\frac{1}{4}\delta_{\rm r} + \frac{\delta\rho_{\rm r} + \delta\rho_{\rm m}}{4\rho_{\rm r} + 3\rho_{\rm m}} = \frac{\rho_{\rm m}}{4\rho_{\rm r} + 3\rho_{\rm m}}\left(\delta_{\rm m} - \frac{3}{4}\delta_{\rm r}\right), \tag{3.30}$$

where we have defined a new parameter, the density contrast δ_i as

$$\delta_i \equiv \frac{\delta\rho_i}{\bar{\rho}_i}. \tag{3.31}$$

Now we define the the entropy perturbation between matter and radiation to be

$$\mathcal{S}_{\rm mr} \equiv \delta_{\rm m} - \frac{3}{4}\delta_{\rm r} = \frac{\delta_{\rm m}}{1+w_{\rm m}} - \frac{\delta_{\rm r}}{1+w_{\rm r}}. \tag{3.32}$$

For matter, or non-relativistic particles, the energy density is just the rest mass times the number density, $\rho_{\rm m} = m n_{\rm m}$. Thus $\delta\rho_{\rm m} \propto \delta n_{\rm m}$ which means $\delta_{\rm m} = \delta\rho_{\rm m}/\rho_{\rm m} = \delta n_{\rm m}/n_{\rm m}$. On the other hand, for the radiation or relativistic particles $\rho_{\rm r} \propto T^4$ and $n_{\rm r} \propto T^3$ [8] giving $\rho_{\rm r} \propto n_{\rm r}^{4/3}$ from which we get $\delta_{\rm r} = 4/3(\delta n_{\rm r}/n_{\rm r})$. Thus the entropy perturbation $\mathcal{S}_{\rm mr}$ can also be written as

$$\mathcal{S}_{\rm mr} = \frac{\delta n_{\rm m}}{n_{\rm m}} - \frac{\delta n_{\rm r}}{n_{\rm r}} = \frac{\delta(n_{\rm m}/n_{\rm r})}{n_{\rm m}/n_{\rm r}}. \tag{3.33}$$

In the early universe our matter species are the baryons (b) and cold dark matter (c) while the radiation consists of photons (γ) and neutrinos (ν). Thus $\rho_{\rm m} = \rho_{\rm b} + \rho_{\rm c}$ and $\rho_{\rm r} = \rho_\gamma + \rho_\nu$. Now the entropy perturbation can be written as

$$\mathcal{S}_{\rm mr} = a_{\rm b}\delta_{\rm b} + a_{\rm c}\delta_{\rm c} + \tfrac{4}{3}(a_\gamma\delta_\gamma + a_\nu\delta_\nu), \tag{3.34}$$

where $a_{\rm b} = \rho_{\rm b}/\rho_{\rm m}$, $a_{\rm c} = \rho_{\rm c}/\rho_{\rm m}$, $a_\gamma = \rho_\gamma/\rho_{\rm r}$ and $a_\nu = \rho_\nu/\rho_{\rm r}$. This then can be put in form

$$\mathcal{S}_{\rm mr} = a_{\rm b}\mathcal{S}_{{\rm b}\gamma} + a_{\rm c}\mathcal{S}_{{\rm c}\gamma} - a_\nu\mathcal{S}_{\nu\gamma}, \tag{3.35}$$

where we have defined the entropy perturbation between to types of particles

$$\mathcal{S}_{\mathrm{ij}} \equiv \frac{\delta_i}{1+w_i} - \frac{\delta_j}{1+w_j} = \frac{\delta n_{\mathrm{i}}}{n_{\mathrm{i}}} - \frac{\delta n_{\mathrm{j}}}{n_{\mathrm{j}}} = -3\mathcal{H}\left(\frac{\delta\rho_i}{\rho_i'} - \frac{\delta\rho_j}{\rho_j'}\right). \tag{3.36}$$

It is sufficient to only consider the entropy perturbation between photons and some other type of particle $\mathcal{S}_{i\gamma}$ since the others can be expressed in terms of these. With this definition, that we shall use, positive entropy perturbation means relative overdensity with respect to photons for the type of particles in question.

In addition to these, there is yet another type of entropy perturbation. It is called the neutrino velocity mode and refers to such a situation, where the rest frame of the neutrino fluid does not coincide with the rest frame on the photon fluid [29].

Comparing the expressions (3.26) and (3.36) we see that our definitions really correspond to entropy perturbations. In this thesis we concentrate on the entropy perturbations in the cold dark matter, thus in our case

$$\mathcal{S} = \mathcal{S}_{\mathrm{c}\gamma} = \delta_{\mathrm{c}} - \frac{3}{4}\delta_\gamma. \tag{3.37}$$

3.1.8 Evolution Equations

Now we have both sides of the Einstein equation and there are equations for the 0-0–, 0-i– and i-j–components. The i-j equation is split into trace and traceless parts

$$3\mathcal{H}(\Psi' + \mathcal{H}\Phi) - \nabla^2\Psi = -4\pi G a^2 \nabla\rho, \tag{3.38}$$

$$(\Psi' + \mathcal{H}\Phi)_{,i} = 4\pi G a^2(\bar{\rho} + \bar{p})v_{,i}, \tag{3.39}$$

$$\Psi'' + \mathcal{H}(\Phi' + 2\psi') + (2\mathcal{H}' + \mathcal{H}^2)\Phi + \tfrac{1}{3}\nabla^2(\Phi - \Psi) = 4\pi G a^2 \delta p, \tag{3.40}$$

$$(\partial_i\partial_j - \tfrac{1}{3}\delta_i^j\nabla^2)(\Psi - \Phi) = 8\pi G a^2 \bar{p}(\partial_i\partial_j - \tfrac{1}{3}\delta_j^i\nabla^2)\Pi. \tag{3.41}$$

The equation (3.41) can be manipulated into the form

$$\Psi - \Phi = 8\pi G a^2 \bar{p}\Pi. \tag{3.42}$$

Since the quantity Π describes the deviation from the perfect fluid, we see that when there is no such deviation the two metric perturbations Φ and Ψ are equal.

The equation (3.39) equation gives

$$\Psi' + \mathcal{H}\Phi = 4\pi G a^2(\bar{\rho} + \bar{p})v. \tag{3.43}$$

Using this with the equation (3.38) we get something reminiscent of the equation for the gravitational potential in Newton's gravity

$$\nabla^2\Psi = 4\pi G a^2 \bar{\rho}[\delta + 3\mathcal{H}(1+w)v], \tag{3.44}$$

where w is the equation-of-state parameter for the whole fluid.

The set of equations simplifies considerably if we take the anisotropic stress to be absent since then $\Phi = \Psi$. The pressure perturbation we get from the definition of the entropy perturbation (3.27)

$$\frac{\delta p}{\rho} = c_{\mathrm{s}}^2[\delta - 3(1+w)\mathcal{S}], \tag{3.45}$$

where $c_{\mathrm{s}}^2 = \bar{p}'/\bar{\rho}'$ is the sound speed of the fluid. Using this and the other evolution equations we get the evolution equation for Ψ

$$\Psi'' + 3\mathcal{H}(1+c_{\mathrm{s}}^2)\Psi' + 3\mathcal{H}^2(c_{\mathrm{s}}^2+w)\Psi - c_{\mathrm{s}}^2\nabla^2\Psi = -\tfrac{9}{2}\mathcal{H}^2 c_{\mathrm{s}}^2(1+w)\mathcal{S}. \tag{3.46}$$

While the entropy perturbation evolves according to

$$\mathcal{S}'' + (1+3c_{\mathrm{z}}^2)\mathcal{H}\mathcal{S}' = -\nabla^2\left(\tfrac{1}{3(1+w)}\delta - c_{\mathrm{z}}^2\mathcal{S}\right), \tag{3.47}$$

where $c_{\mathrm{z}}^2 = \frac{y}{3y+4}$, $y = \frac{a}{a_{\mathrm{eq}}}$ and a_{eq} is the scale factor at the time of matter-radiation–equality[2].

Fourier Modes

Usually, it is more convenient to work in Fourier space than in coordinate space. With cosmological perturbations this is especially true. Since we Fourier expand the spatial dependence, and the only spatial dependence we have is in the perturbed quantities, all our Fourier components are perturbations. Thus, to first order, there is no mixing between the different Fourier modes and each one of them evolves independently of one another.

Additionally, we can now classify the evolution, according to the relation of the wavelength to the horizon, to sub- and superhorizon ones when $k > \mathcal{H}$ and $k < \mathcal{H}$, respectively.

In Fourier space the equations (3.46) and (3.47) read

$$\mathcal{H}^{-2}\Psi_{\mathbf{k}}'' + 3\mathcal{H}^{-1}(1+c_{\mathrm{s}}^2)\Psi_{\mathbf{k}}' + 3(c_{\mathrm{s}}^2+w)\Psi_{\mathbf{k}} + c_{\mathrm{s}}^2\tfrac{k^2}{\mathcal{H}^2}\Psi_{\mathbf{k}} = -\tfrac{9}{2}c_{\mathrm{s}}^2(1+w)\mathcal{S}_{\mathbf{k}} \tag{3.48}$$

$$\mathcal{H}^{-2}\mathcal{S}_{\mathbf{k}}'' + (1+3c_{\mathrm{z}}^2)\mathcal{H}^{-1}\mathcal{S}_{\mathbf{k}}' = \tfrac{k^2}{\mathcal{H}^2}\left(\tfrac{1}{3(1+w)}\delta - c_{\mathrm{z}}^2\mathcal{S}_{\mathbf{k}}\right). \tag{3.49}$$

We see that the entropy perturbation $\mathcal{S}$ is a source term for the curvature perturbation Ψ and thus also for $\mathcal{R}$, which is a function of Ψ. For entropy perturbations, the source term vanishes while the modes are outside the horizon since then $\frac{k^2}{\mathcal{H}^2} \ll 1$.

Calculating $\mathcal{R}'$ we see that $\mathcal{R}' = 0$ is equivalent to the equation (3.48) when there is no entropy perturbation and the mode is outside the horizon [26]. Thus the curvature perturbation stays constant on superhorizon scales in the absence of entropy perturbations. Actually, the conservation of the curvature perturbations is valid also beyond first order [30].

Since we are working in first order, the evolution equations are linear and therefore we can write

$$\begin{bmatrix}\mathcal{R}(\eta,\mathbf{k})\\ \mathcal{S}(\eta,\mathbf{k})\end{bmatrix} = \begin{bmatrix}1 & T_{\mathcal{R}\mathcal{S}}(\eta,k)\\ 0 & T_{\mathcal{S}\mathcal{S}}(\eta,k)\end{bmatrix}\begin{bmatrix}\mathcal{R}(\eta_*,\mathbf{k})\\ \mathcal{S}(\eta_*,\mathbf{k})\end{bmatrix}, \tag{3.50}$$

[2]When doing perturbation theory, instead of setting $a(t_0) = 1$ one convenient choice is to define $a(t_{\mathrm{eq}}) = 1$.

where $T_{\mathcal{RS}}(k)$ and $T_{\mathcal{SS}}(k)$ are called the transfer functions and encode the evolution of the perturbations according to the equations (3.48) and (3.49). The quantities $\mathcal{R}(\eta_*, \mathbf{k})$ and $\mathcal{S}(\eta_*, \mathbf{k})$ are the initial values for the perturbations specified at some early time η_* when they were generated in the first place.

The continuously improving quality of the data has led to a situation where it might no longer suffice to study the perturbations at first order only. That analysis quickly becomes very complicated technically [31] as scalar, vector and tensor modes no longer evolve independently and neither do the Fourier modes. In this case, a non-perturbative approach has been studied as more suitable approach [32, 33, 34].

The Initial Values $\mathcal{R}_*$ and $\mathcal{S}_*$

The initial values for the perturbation quantities depends on the model by which they are produced. In the case of inflation, the perturbations arise from the quantum fluctuations of the inflaton field:

$$\varphi(\eta, \mathbf{k}) = \bar{\varphi}(\eta) + \delta\varphi(\eta, \mathbf{k}). \tag{3.51}$$

When considering inflation, there is a crucial difference between single- and multi-field inflation. With single-field there is only one degree of freedom, the inflaton field φ. In this case only curvature perturbations can be produced and we have [35]

$$\mathcal{R}_*(\mathbf{k}) = \mathcal{R}(\eta_*, \mathbf{k}) = -\frac{\mathcal{H}}{\varphi'}\delta\varphi_{\mathbf{k}}, \quad \text{with} \quad \delta\varphi_{\mathbf{k}} \propto \hat{e}(\mathbf{k}). \tag{3.52}$$

The expression is evaluated as the mode in question crosses the horizon, i.e., $k = \mathcal{H}$, and $\hat{e}(\mathbf{k})$ is a Gaussian random variable with zero mean and unit variance.

If there are more than one relevant field during inflation, i.e., there is more than one degree of freedom, then it is also possible to produce entropy perturbations. For an example of this in context of two fields, see [36, 37].

Since we wish to keep our analysis as general as possible, we only specify the statistical nature of the perturbations, which we take to be Gaussian with zero mean, unit variance and independent of one another while leaving the amplitude as a free parameter. Thus we have

$$\begin{matrix} \mathcal{R}(\eta_*, \mathbf{k}) \propto \hat{e}_{\mathrm{r}} \\ \mathcal{S}(\eta_*, \mathbf{k}) \propto \hat{e}_{\mathrm{s}} \end{matrix} \quad \text{with} \quad \begin{matrix} \langle \hat{e}_{\mathrm{r}} \rangle = 0 \\ \langle \hat{e}_{\mathrm{s}} \rangle = 0 \end{matrix} \quad \langle \hat{e}_{\mathrm{r}} \hat{e}_{\mathrm{s}}^* \rangle = \delta_{\mathrm{rs}}. \tag{3.53}$$

Adiabatic and Isocurvature Perturbations

Instead of referring to curvature and entropy perturbations, we define adiabatic and isocurvature perturbations. General perturbation can be specified by giving $\mathcal{R}$ and $\mathcal{S}$. The adiabatic mode is initially completely characterised by $\mathcal{R}$ while $\mathcal{S} = 0$. The isocurvature perturbation is the opposite, with $\mathcal{S} \neq 0$ and $\mathcal{R} = 0$. To emphasise, this distinction holds only for the initial condition, as the situation changes in time as seen from the equations (3.48) and (3.49).

3.2 The CMB in the Sky

Now we know how the small deviations from the isotropic and homogeneous background evolve. However, this in itself is not yet enough to find out what we can actually observe, that is the temperature anisotropies in the CMB. To begin with, we do not have enough information, we have 4 evolution equations, but 6 quantities, δ, δp, v, Π, Ψ and Φ in the full case and one equation and two quantities less if we make the perfect fluid approximation.

Also missing is the interaction between different types of energy. The Einstein equations describe only the effect of gravity. The dark energy does not have any interactions and contributes only to and via gravity. At $T \sim 1$ MeV neutrinos have decoupled from photons, so they too only contribute to the energy density. What is left then is the Compton scattering between photons and baryons.

3.2.1 Temperature and Polarisation Anisotropy

The obvious and simple observables are the temperature anisotropies of the CMB. This is nothing but the angular dependence in the temperature on the measured CMB, originally sourced by the small deviations from the smooth background discussed above.

In addition to the simple temperature anisotropies the CMB radiation is also linearly polarised due to Thomson scattering. The polarisation is slightly more complex to handle than the temperature anisotropies but the generation of the polarisation in the first place is a rather simple process to follow.

Thomson Scattering

The polarisation is generated by the Thomson scattering of photons from electrons. Thomson scattering is the Compton scattering at the limit when there is no energy transfer to photons and only the photon direction changes. The scattering produces polarisation since the differential cross section of Thomson scattering depends on polarisations $\hat{\epsilon}'$ and $\hat{\epsilon}$ of the incident and scattered photons

$$\frac{d\sigma}{d\Omega} = \frac{3\sigma_{\mathrm{T}}}{8\pi}|\hat{\epsilon}' \cdot \hat{\epsilon}|^2. \tag{3.54}$$

We see that the scattering is strongest when the polarisation of incident and scattered radiation are parallel and there is no scattering when they are perpendicular.

To get the overall polarisation scattered in a given direction one needs to integrate over all incoming directions. If the incident radiation is completely isotropic, then the polarisation generated by the scattering evens out and we get unpolarised radiation. In order for the scattered radiation to be polarised the incident radiation must be anisotropic, which it naturally is. The exact calculation gives that the incident radiation must possess a quadrupole anisotropy for the outgoing radiation to be polarised [38, 39].

Amount of Polarisation

A quadrupole anisotropy can be generated at around recombination when the photons decouple from electrons. Before that, the constant rescatterings erase any generated quadrupole. Thus the window to generate the polarisation is not too long, since while the recombination proceeds the electrons and nuclei form neutral atoms and the free electron density decreases, reducing the scatterings that produce the polarisation.

This generating process makes the polarisation sensitive to the ionisation history of the universe. The downside is that the amplitude of polarised anisotropy is small, $\sim$10% of the temparature anisotropies at best [39] making the observational aspect of polarisation quite challenging.

E- and B-mode Polarisation

Unlike the temperature anisotropy which is a scalar, the linear polarisation can be described a pseudo-vector, meaning that it has magnitude and orientation. The temperature anisotropy is analysed in terms of spherical harmonics while for the polarisation we must employ either spin-2 spherical harmonics [40] or, alternatively, tensor spherical harmonics [41]. Both of these methods lead to the same result. This can then in the end be expressed in terms of two scalar fields, that are called the E-mode and the B-mode.

This division turns out to be very useful. The E-mode is generated by the scalar, vector and tensor perturbations. However, the vector perturbations are taken to be absent and the tensor perturbations are small in comparison with the scalar ones and thus, for practical purposes, the E-mode comes from the scalar perturbations. Even more interesting part is the B-mode. That is sourced by both vector and tensor perturbations, but since the vector part is absent, the B-mode comes from the tensor perturbations alone. This makes the measurement of the B-mode extremely appealing, since it is the best probe for tensor perturbations [42, 43]. Unfortunately, exactly because of the low amplitude of tensor perturbations, the B-mode is yet to be detected.

Another added subtlety is the conversion of the E-mode polarisation to B-mode by the gravitational lensing by the clusters of galaxies [44, 45]. Thus a B-mode polarisation exists for sure, even in the absence of tensor perturbations. Fortunately, the primordial B-mode, produced by the tensor perturbations, peaks at different scales than the one produced by the lensing so these effects should be separable. This effect also works the other way around, converting B-mode to E-mode, but since the amplitude of the B-mode is so small to begin with, this effect is extremely small.

3.2.2 Boltzmann Equation

What we need for a more thorough analysis, is the distribution function for a species of particles $f = f(\eta, x^i, q^i)$, which gives the phase space distribution of the particles in question:

$$dN = f(\eta, x^i, q^i) d^3x d^3q. \tag{3.55}$$

From the distribution function we get the energy density, pressure and momentum flux, i.e., the components of the energy tensor

$$\begin{aligned} \bar{\rho} + \delta\rho &= \int E(q) f d^3q, & \Pi &= \bar{p} \int (q^i q^j - \tfrac{1}{3}\delta^{ij} q^2) \frac{f d^3q}{E(q)}, \\ \bar{p} + \delta p &= \int \frac{\delta_{ij} q^i q^j}{3E(q)} f d^3q, & (\bar{\rho} + \bar{p}) v_i &= \int q^i f d^3q. \end{aligned} \tag{3.56}$$

The additional information to describe the system in more detail is then given by the Boltzmann equation which governs the evolution of the distribution function

$$\frac{df}{d\eta} = C[f]. \tag{3.57}$$

The term $C[f]$ is the collision term describing the interactions between the particles. The full details from obtaining the angular power spectrum starting from the distribution function can be found, for example, in [38].

Brightness Function

Since our interacting component is the photons and they is what we eventually observe, we need the distribution function for photons. For the background universe, assuming thermal equilibrium is a valid approximation, we have the familiar Bose-Einstein distribution function

$$f_{\rm eq}(\eta, x^i, q^i) = \bar{f}(\eta, q^i) = \frac{g}{(2\pi)^3} \frac{1}{e^{q/T} - 1}, \tag{3.58}$$

where g is the number of internal degrees of freedom and for photons it is 2. Let us now introduce a small perturbation to the background by making the temperature anisotropic but maintaining local thermal equilibrium. Thus the perturbed distribution function is

$$f(\eta, x^i, q^i) = \frac{g}{(2\pi)^3} \frac{1}{\exp\left\{ \frac{q}{T(\eta)[1+\Theta(\eta, x^i, q^i)]} \right\} - 1}. \tag{3.59}$$

We have introduced a function Θ, called the brightness function, to define the anisotropy in the temperature, through

$$T(\eta, x^i, q^i) = T(\eta)[1 + \Theta(\eta, x^i, q^i)]. \tag{3.60}$$

Writing the temperature as $T = \bar{T} + \Delta T$, we see that the brightness function can also be thought of as the relative temperature perturbation

$$\Theta = \frac{\Delta T}{\bar{T}}. \tag{3.61}$$

It turns out that the brightness function is independent of the magnitude of q^i in first order perturbation theory and thus only depends on the direction $\hat{n}$ of q^i [38]

$$\Theta(\eta, x^i, q^i) = \Theta(\eta, x^i, \hat{n}). \tag{3.62}$$

.

3.2.3 Angular Power Spectra

What we observe is, as already stated, the temperature anisotropy on the sky today, i.e.,

$$\frac{\Delta T}{T}(\eta_0, x^i, \hat{n}) = \Theta(\eta_0, x^i, \hat{n}). \tag{3.63}$$

The anisotropy is a function of time and space, but in practice we can only make observations on a single point in spacetime, here and now. Should we be able to make observations on scales that are not insignificant compared with Hubble length and time, we should expect to see variation in Θ. Since this is not the case, all the information we get out of Θ is in its angular dependence. Thus we simply denote

$$\Theta(\eta_0, x^i, \hat{n}) = \Theta(\hat{n}), \tag{3.64}$$

where we have chosen $x^i = 0$ for simplicity.

Since the temperature anisotropy is now just a function on the sky, we expand it in terms of spherical harmonics

$$\Theta(\hat{n}) = \sum_{lm} a_{lm} Y_{lm}(\hat{n}). \tag{3.65}$$

The multipole coefficients a_{lm} can then be simply obtained by the orthogonality of the spherical harmonics

$$a_{lm} = \int d\Omega \Theta(\hat{n}) Y^*_{lm}(\hat{n}) = (2\pi)^{-\frac{3}{2}} \int d\Omega d^3k \Theta(\hat{n}, \mathbf{k}) Y^*_{lm}(\hat{n}), \tag{3.66}$$

where the latter form just comes from the inverse Fourier transformation with $e^{i\mathbf{k}\cdot\mathbf{x}} = 1$ since we chose $\mathbf{x} = 0$.

The angular power spectrum C_l is defined as the variance of the multipole coefficients a_{lm}, i.e.,

$$C_l \equiv \langle a_{lm} a^*_{lm} \rangle. \tag{3.67}$$

The angular power spectrum is independent of m meaning that only the angular scale of the anisotropy matters not its orientation. Thus we have

$$C_l = \int d\Omega d\Omega' Y^*_{lm}(\hat{n}) Y_{lm}(\hat{n}') (2\pi)^{-3} \int d^3k d^3k' \langle \Theta(\hat{n}, \mathbf{k}) \Theta^*(\hat{n}', \mathbf{k}') \rangle. \tag{3.68}$$

Now $\Theta(\hat{n}, \mathbf{k})$ is the Fourier mode of the temperature perturbation and its evolution is given by the Boltzmann equation. Since we are working with first order perturbations the evolution equations are linear and we can write similarly as we did for the perturbed Einstein equations:

$$\Theta(\eta_0, \hat{n}, \mathbf{k}) = g(\eta_0, \hat{n}, k) X(\eta_{\text{init}}, \mathbf{k}), \tag{3.69}$$

where $g(\eta_0, \hat{n}, k)$ is the transfer function encoding the evolution of the perturbations from the initial time η_{init} to today and $X(\eta_{\text{init}}, \mathbf{k})$ is a quantity characterising the perturbation at the initial time. We wrote the times explicitly to emphasise when the quantities are defined. We note that the transfer functions are functions of the magnitude k, but not the direction, of $\mathbf{k}$ meaning that the Boltzmann equation does not have a preferred direction.

Now we need the correlator for the initial perturbations $X(\eta_{\rm init}, \mathbf{k}) = X(\mathbf{k})$. For a process that is isotropic and Gaussian, the different Fourier modes are independent and the correlation only depends on the magnitude of $\mathbf{k}$:

$$\langle X(\mathbf{k}) X^*(\mathbf{k}')\rangle = \frac{2\pi^2}{k^3}\mathcal{P}_X(k)\delta^{(3)}(\mathbf{k}-\mathbf{k}'), \tag{3.70}$$

where $\mathcal{P}_X(k)$ is called the power spectrum of X.

Inserting (3.69) into (3.68) and using the correlation (3.70) we get, after intergrating over $\mathbf{k}'$,

$$C_l = \int d\Omega d\Omega' Y^*_{lm}(\hat{n}) Y_{lm}(\hat{n}') \int \frac{dk}{k} g(\eta_0, k, \hat{n}) g^*(\eta_0, k', \hat{n}') \mathcal{P}_X(k). \tag{3.71}$$

Let us then expand the transfer functions in terms of spherical harmonics:

$$g(\eta_0, k, \hat{n}) = \sum_{l'm'} g_{l'm'}(\eta_0, k) Y_{l'm'}(\hat{n}). \tag{3.72}$$

Inserting this into the expression for C_l and performing the two angular integrations we obtain

$$C_l = \int \frac{dk}{k} |g_{lm}(\eta_0, k)|^2 \mathcal{P}_X(k) = \int \frac{dk}{k} g_l^2(\eta_0, k) \mathcal{P}_X(k). \tag{3.73}$$

The last expression in (3.73) follows from the fact that the transfer functions are real and the orientation is included in the transfer functions (essentially there is a sum over all m).

Angular Power Spectra for the General Case

The expression (3.73) gives the angular power spectrum of the temperature anisotropies. The result for the polarisation and temperature-polarisation crosscorrelation is formally the same. In our case we are studying the isocurvature perturbations as well, so next we present the expression (3.73) generalised to include polarisation and both adiabatic and isocurvature perturbations.

The correlation for a more generic case of initial perturbations is given by

$$\langle X(\eta_{\rm init}, \mathbf{k}) Y^*(\eta_{\rm init}, \mathbf{k}')\rangle = \frac{2\pi^2}{k^3}\mathcal{C}_{XY}(\eta_{\rm init}, k)\delta^{(3)}(\mathbf{k}-\mathbf{k}'), \tag{3.74}$$

where X and Y are the initial perturbations and can include any combination adiabatic and isocurvature modes. In case of autocorrelation the correlator $\mathcal{C}_{XX}$ is called the power spectrum and usually denoted by $\mathcal{P}_X$. The assumption that the initial perturbations are produced by a isotropic Gaussian process applies here as well.

The total angular power spectra is then given by

$$C_l^{\rm ab} = \sum_{XY} \int \frac{dk}{k} \mathcal{C}_{XY}(\eta_{\rm init}, k) g^{\rm a}_{Xl}(k) g^{\rm b}_{Yl}(k). \tag{3.75}$$

The indices a and b denote temperature T or polarisation E/B anisotropies and the sum goes over all combinations. The transfer functions $g^{\rm a}_{Xl}(k)$ are separate for temperature and polarisation, denoted by the index a, and describe how a perturbation of type X evolves from the initial time $\eta_{\rm init}$ to today η_0.

For the calculation of the CMB anisotropies, the initial time is when the universe was still deep in the radiation dominated era and all of the cosmologically interesting scales, i.e., the ones we can observe today, are well outside the horizon. It is, however, after the nucleosynthesis so the temperature is around $T \sim 0.1\,\mathrm{MeV}$. Thus the energy menu consists of photons, neutrinos, baryons and cold dark matter. The dark energy we take to be the cosmological constant which does not have perturbations and therefore affects the background evolution only. We denote this time as η_{rad}.

As mentioned above, there is an emerging need to study the perturbations beyond first order in the perturbative expansion. Since the CMB is what we actually observe, also the Boltzmann equation needs to be expanded to second order. This also becomes technically very complicated [46, 47] as well as computationally more challenging and currently there are no, at least not publicly available, implementations that could produce the CMB anisotropies to second order.

3.2.4 Angular Power Spectra in Our Analysis

The equation (3.50) at the initial time $\eta_{\mathrm{init}} = \eta_{\mathrm{rad}}$ reads

$$\begin{bmatrix} \mathcal{R}(\eta_{\mathrm{rad}}, \mathbf{k}) \\ \mathcal{S}(\eta_{\mathrm{rad}}, \mathbf{k}) \end{bmatrix} = \begin{bmatrix} 1 & T_{\mathcal{RS}}(k) \\ 0 & T_{\mathcal{SS}}(k) \end{bmatrix} \begin{bmatrix} \mathcal{R}(\eta_*, \mathbf{k}) \\ \mathcal{S}(\eta_*, \mathbf{k}) \end{bmatrix}, \tag{3.76}$$

where the transfer functions $T_{XY}(\eta_{\mathrm{rad}}, k) = T_{XY}(k)$ encode the evolution from the generated perturbations to our initial time of η_{rad}. As stated before we take the perturbations to be produced by a isotropic Gaussian process in such a way that they are initially uncorrelated.

With the equation above and the definitions (3.53) the correlator (3.74) gives

$$\mathcal{C}_{\mathcal{RR}}(\eta_{\mathrm{rad}}, k) = \mathcal{P}_{\mathcal{R}}(\eta_*, k) + T^2_{\mathcal{RS}}(k)\mathcal{P}_{\mathcal{S}}(\eta_*, k), \tag{3.77}$$

$$\mathcal{C}_{\mathcal{RS}}(\eta_{\mathrm{rad}}, k) = T_{\mathcal{RS}}(k)T_{\mathcal{SS}}(k)\mathcal{P}_{\mathcal{S}}(\eta_*, k), \tag{3.78}$$

$$\mathcal{C}_{\mathcal{SS}}(\eta_{\mathrm{rad}}, k) = T^2_{\mathcal{SS}}(k)\mathcal{P}_{\mathcal{S}}(\eta_*, k), \tag{3.79}$$

where $\mathcal{P}_{\mathcal{R}}(\eta_*, k)$ and $\mathcal{P}_{\mathcal{S}}(\eta_*, k)$ are the power spectra of the generated adiabatic and isocurvature perturbations. We now see that the adiabatic mode $\mathcal{C}_{\mathcal{RR}}$ is actually formed out of two parts, the original generated adiabatic perturbation and the adiabatic perturbation sourced by the isocurvature perturbation. The isocurvature part $\mathcal{C}_{\mathcal{SS}}$ is only sourced by the original generated isocurvature perturbation. There is also a correlation between the adiabatic and isocurvature perturbation $\mathcal{C}_{\mathcal{RS}}$ since they partially share the same source.

The exact form of the power spectra and the transfer functions is model dependent. In order to be able to calculate the CMB angular power spectra we need to approximate the transfer functions and power spectra, which we now assume to take the following form

$$\begin{aligned} \mathcal{P}_{\mathcal{R}}(t_*, k) &\propto k^{m_1} \\ \mathcal{P}_{\mathcal{S}}(t_*, k) &\propto k^{m_2} \end{aligned} \quad \text{and} \quad \begin{aligned} T_{\mathcal{RS}}(k) &\propto k^{m_3} \\ T_{\mathcal{SS}}(k) &\propto k^{m_4} \end{aligned} \tag{3.80}$$

This and the statistical nature are the only approximations that we make regarding the origin of perturbations. The results from the analysis are applicable for any model for which this approximation applies.

With the above power law approximation the autocorrelations are

$$\begin{aligned}\mathcal{P}_{\mathcal{R}}(\eta_{\rm rad},k) &= \mathcal{C}_{\mathcal{R}\mathcal{R}}(\eta_{\rm rad},k) = A_r^2\left(\frac{k}{k_0}\right)^{n_{\rm ad1}-1} + A_s^2\left(\frac{k}{k_0}\right)^{n_{\rm ad2}-1},\\ \mathcal{P}_{\mathcal{S}}(\eta_{\rm rad},k) &= \mathcal{C}_{\mathcal{S}\mathcal{S}}(\eta_{\rm rad},k) = B^2\left(\frac{k}{k_0}\right)^{n_{\rm iso}-1},\end{aligned} \tag{3.81}$$

where k_0 is the scale at which the amplitudes, A_r, A_s and B are defined. We have chosen this scale, called the pivot scale, to be $k_0 = 0.01\,\mathrm{Mpc}^{-1}$. We also comment on the effects of this choice in the analysis in section 4. The spectral indices are

$$\begin{aligned}n_{\rm ad1} &= m_1 + 1,\\ n_{\rm ad2} &= m_2 + 2m_3 + 1,\\ n_{\rm iso} &= m_2 + 2m_4 + 1.\end{aligned} \tag{3.82}$$

If we would only consider adiabatic perturbations, then only the first term of first equation would exist and the spectral index $n_{\rm ad1}$ would be the usual adiabatic spectral index. The presence of a correlated isocurvature perturbation means that we can not characterise the adiabatic spectra by just a single spectral index.

The crosscorrelation between the second adiabatic and the isocurvature mode is

$$\mathcal{C}_{\mathcal{R}\mathcal{S}}(\eta_{\rm rad},k) = \mathcal{C}_{\mathcal{S}\mathcal{R}}(\eta_{\rm rad},k) = A_s B\left(\frac{k}{k_0}\right)^{n_{\rm cor}-1}, \tag{3.83}$$

where the correlation spectral index is not an independent parameter but

$$n_{\rm cor} = m_2 + m_3 + m_4 + 1 = \frac{1}{2}(n_{\rm ad2} + n_{\rm iso}). \tag{3.84}$$

Now using the equation (3.75) with (3.81) and (3.83) we get the expression for the temperature and E-mode polarisation angular power spectrum:

$$\begin{aligned}C_l^{\rm AA} &= \int \frac{dk}{k}\big[A_r^2 (g^{\rm A}_{\mathcal{R}l})^2 \tilde{k}^{n_{\rm ad1}-1} + A_s^2 (g^{\rm A}_{\mathcal{R}l})^2 \tilde{k}^{n_{\rm ad2}-1}\\ &\quad + B^2 (g^{\rm A}_{\mathcal{S}l})^2 \tilde{k}^{n_{\rm iso}-1} + 2A_s B g^{\rm A}_{\mathcal{R}l} g^{\rm A}_{\mathcal{S}l} \tilde{k}^{n_{\rm cor}-1}\big]\\ &\equiv A_r^2 \hat{C}_l^{\rm AAad1} + A_s^2 \hat{C}_l^{\rm AAad2} + B^2 \hat{C}_l^{\rm AAiso} + A_s B \hat{C}_l^{\rm AAcor},\end{aligned} \tag{3.85}$$

where A denotes either temperature, T, or E-mode polarisation, E, and we use the shorthand notation $\tilde{k} = k/k_0$. The temperature-polarisation crosscorrelation angular power spectra is

$$\begin{aligned}C_l^{\rm TE} &= \int \frac{dk}{k}\big[A_r^2 g^{\rm T}_{\mathcal{R}l} g^{\rm E}_{\mathcal{R}l} \tilde{k}^{n_{\rm ad1}-1} + A_s^2 g^{\rm T}_{\mathcal{R}l} g^{\rm E}_{\mathcal{R}l} \tilde{k}^{n_{\rm ad2}-1}\\ &\quad + B^2 g^{\rm T}_{\mathcal{S}l} g^{\rm E}_{\mathcal{S}l} \tilde{k}^{n_{\rm iso}-1} + A_s B (g^{\rm T}_{\mathcal{R}l} g^{\rm E}_{\mathcal{S}l} + g^{\rm T}_{\mathcal{S}l} g^{\rm E}_{\mathcal{R}l}) \tilde{k}^{n_{\rm cor}-1}\big]\\ &\equiv A_r^2 \hat{C}_l^{\rm TEad1} + A_s^2 \hat{C}_l^{\rm TEad2} + B^2 \hat{C}_l^{\rm TEiso} + A_s B \hat{C}_l^{\rm TEcor}.\end{aligned} \tag{3.86}$$

Thus we now have three separate amplitude parameters to use in the analysis. The simplest choice would just use A_r, A_s and B as such. However, this is not the best choice as we would prefer to have

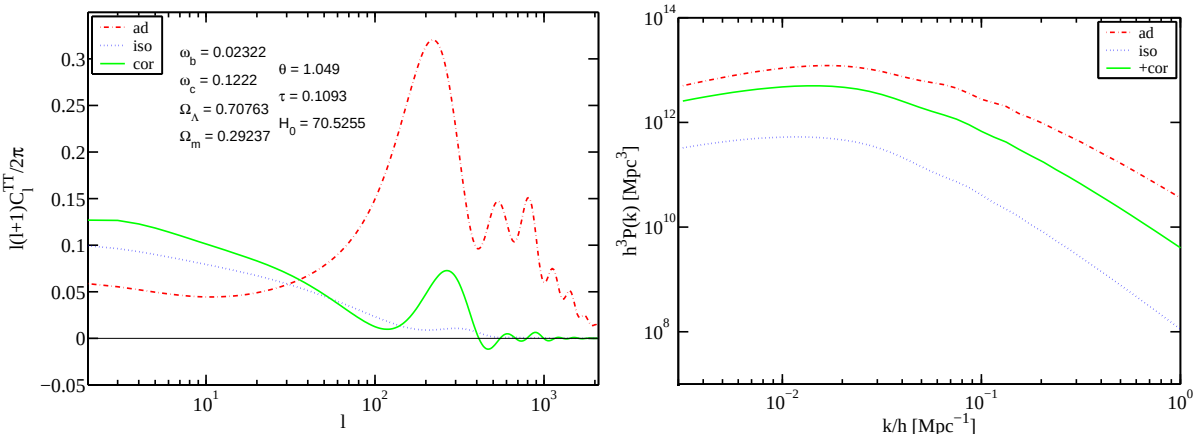

Figure 3.1: Components of the angular power spectrum and the matter power spectrum with unit amplitudes. Figure from [2].

one overall amplitude and then relative contributions to the isocurvature and correlation parts. In the end, there is no best choice of parametrisation and we will discuss this more in the next chapter.

In addition to the above, we prefer such an amplitude parametrisation for which the data has a linear response. Thus we define the overall amplitude A as

$$A^2 \equiv A_r^2 + A_s^2 + B^2 \tag{3.87}$$

and the isocurvature fraction and the degree of correlation as

$$\alpha \equiv \frac{B^2}{A^2} \quad \text{with} \quad \alpha \in [0,1], \tag{3.88}$$

$$\gamma \equiv \text{sign}(A_s B)\frac{A_s^2}{A_r^2 + A_s^2} \quad \text{with} \quad \gamma \in [-1,1]. \tag{3.89}$$

With these parameters the total angular power spectrum can be written as:

$$\begin{aligned} C_l &= A^2[(1-\alpha)(1-|\gamma|)\hat{C}_l^{\text{ad1}} + (1-\alpha)|\gamma|\hat{C}_l^{\text{ad2}} + \alpha\hat{C}_l^{\text{iso}} \\ &\quad + \text{sign}(\gamma)\sqrt{\alpha(1-\alpha)|\gamma|}\hat{C}_l^{\text{cor}} \\ &\equiv C_l^{\text{ad1}} + C_l^{\text{ad2}} + C_l^{\text{iso}} + C_l^{\text{cor}}. \end{aligned} \tag{3.90}$$

The quantities $\hat{C}_l^{\text{ad1}}$ and $\hat{C}_l^{\text{ad2}}$ are the adiabatic spectra that would result from a curvature perturbation $\mathcal{R}(\eta_{\text{rad}})$ with unit amplitude, i.e., $A_r = 1$ or $A_s = 1$. They are otherwise exactly the same, but have their own spectral indices n_{ad1} and n_{ad2}, respectively. Likewise, $\hat{C}_l^{\text{iso}}$ is the isocurvature spectrum from the entropy perturbation $\mathcal{S}(\eta_{\text{rad}})$ with unit amplitude $B = 1$ and the correlation $\hat{C}_l^{\text{cor}}$ the contribution with $A_s B = 1$. Figure 3.1 shows the components for the temperature spectrum for such a case.

3.2.5 Matter Power Spectrum

In addition to the distribution of photons, one can also track the inhomogeneities in the matter distribution, which is effectively the cold dark matter distribution since that constitutes most of the

matter density [13]. A relation similar to (3.90) holds also to the matter power spectrum, the unit amplitude example of which is shown in figure 3.1.

The observations for the matter power spectrum come from the galaxy redshift surveys [5]. The galaxies track the distribution of the dark matter which has been decoupled from other particle species for a long time. Thus it has had time to form the gravitational wells where the baryonic matter has subsequently fallen. The redshift surveys probe the three-dimensional distribution of the galaxies and therefore the matter power spectrum is given as two point correlator in the Fourier space insted of in harmonic space as the CMB anisotropies.

Chapter 4

Analysing the Cosmic Microwave Background

Until now we have presented the theoretical framework for how the initial perturbations evolve to form the present observable CMB anisotropies. In this chapter we discuss what data is available, how it is analysed and what are the limits on the isocurvature contribution.

Unfortunately there are no exact analytical expressions for the angular power spectra. Under various approximations one gets reasonably good analytical results which are beneficial to see how the features in the spectra come about. In order to make comparisons to the available data, the analytical results are not accurate enough and one has to resort to numerical calculations. Fortunately there is a selection of freely available codes to calculate the CMB spectra, such as CMBFAST [48], CMBEASY [49] and CAMB [50], which is the one we use in our analysis. The Markov chains are created and analysed using CosmoMC [51].

4.1 CMB Observations

The story of successful CMB measurements begun in 1965 when Penzias and Wilson detected the remnant radiation for the first time. As it occasionally happens in science, this was an accidental discovery. Penzias and Wilson were interested in radio astronomy, not cosmology, and the uniform excess noise from the sky they observed was a worrying problem for them. Eventually, they resolved that it was not a question of, say "white dielectric material" by pigeons living in the antenna, but rather a new discovery for which they received the Nobel price in 1978.

Obviously, the first measurement only detected the isotropic part of the CMB radiation leaving the anisotropies for the future. Nonetheless, it proved that there was indeed something to measure and in the ensuing years there was no lack of efforts to measure the deviation from homogeneity, as seen in the background of the figure 4.1.

It was not until almost three decades later in 1992, when the results from the COBE satellite were published [52], that the anisotropies in the CMB were finally observed for the first time. COBE had

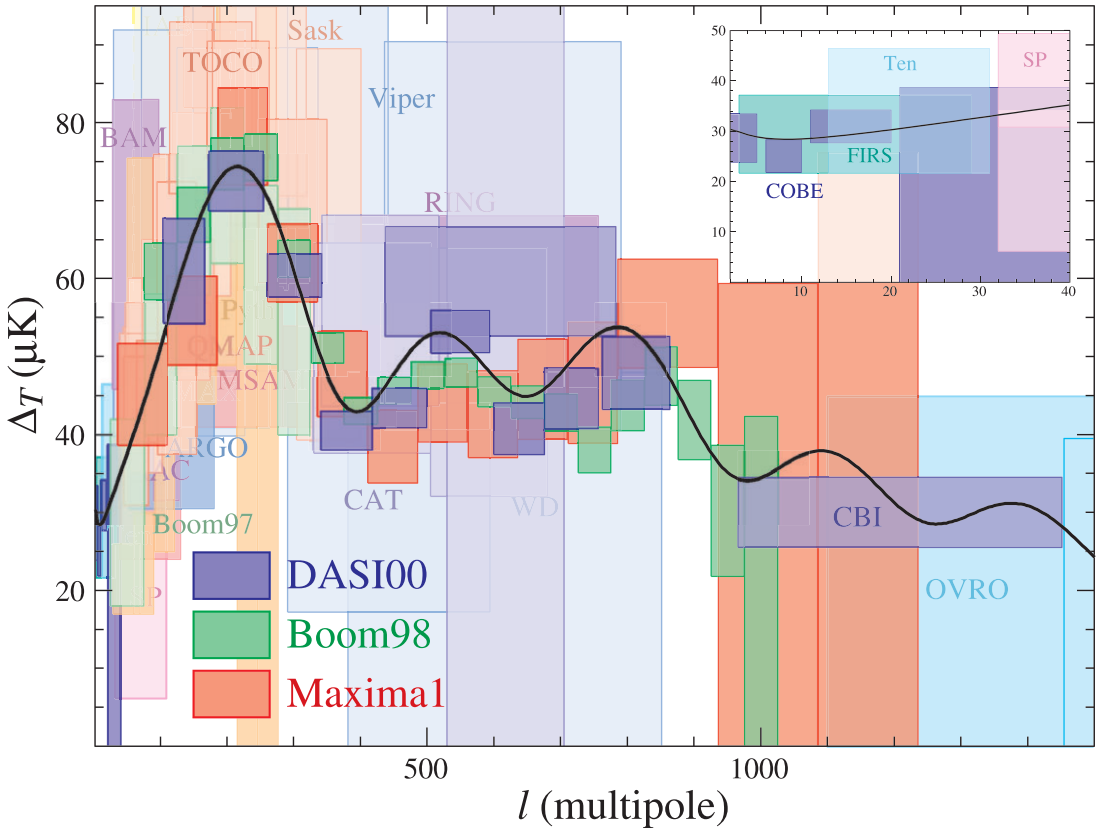

Figure 4.1: Various CMB measurements with corresponding errors. The inset shows the measurements for the lowest multipoles. Figure from [45]

an angular resolution of about 7 degrees, meaning that it was not able to detect structure on smaller scales than that. Since the horizon at the time of last scattering is subtends about one degree in the sky, COBE could only observe superhorizon scales. Thus the most interesting features of the CMB still remained hidden. Nonetheless, this measurement found out that the deviation from the homogeneity was at the 10^{-5} scale.

The measurements that began seeing more structure, specifically the first acoustic peak, in the angular power spectrum were Boomerang [53] and MAXIMA-1 [54] in 2000. Unlike COBE, these were balloon-borne experiments that made their observations high in the Earth's atmosphere.

Nowadays the most important source of CMB data is the WMAP satellite which has been taking data since 2001 is still in operation and is expected to run at least until 2009. Thus far the WMAP team has made three data releases, for 1-year [55], for 3-years [56] and, just recently, for 5-years [13] of observations. Naturally, this is also the main data source in our studies, where we use the 1- and 3-year data sets. The increase in the accuracy from the first Boomerang observations to the current WMAP results is obvious in figure 4.2.

In addition to the accurate temperature anisotropy measurements, the WMAP provides usable polarisation data as well. The first detection of a polarisation signal was, however, not done by WMAP but instead by DASI [57], which is a ground-based instrument operating at the south-pole.

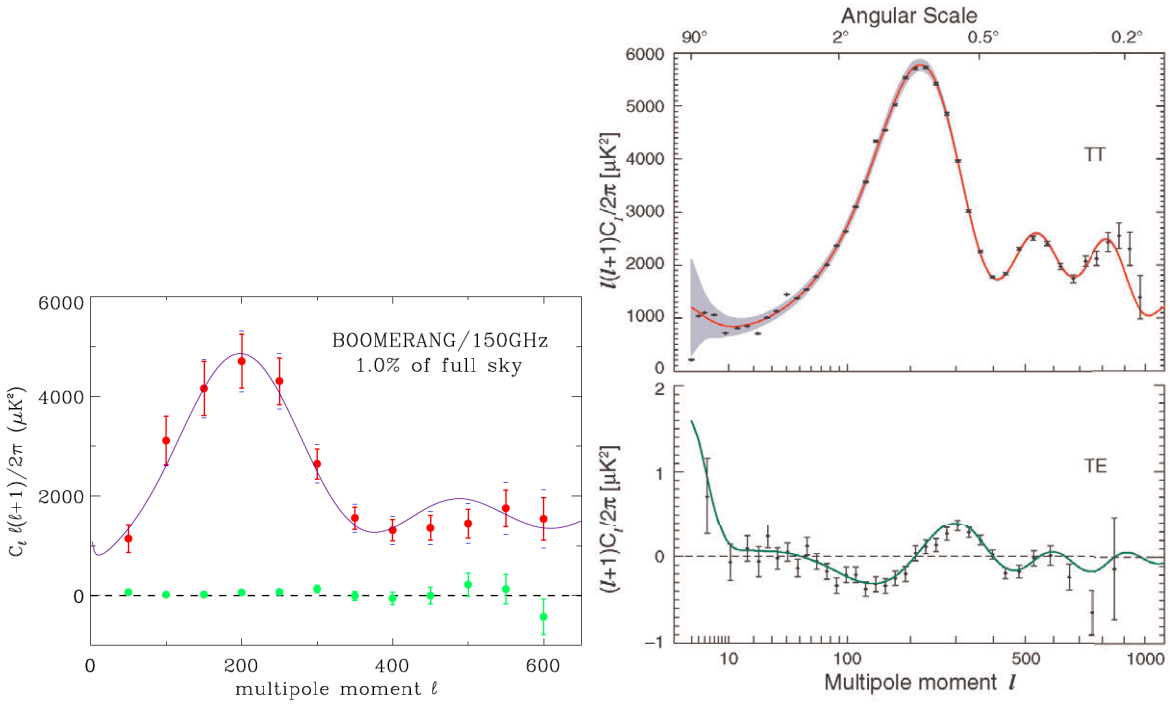

Figure 4.2: The angular power spectra for the first Boomerang data release on the left and for 5-year WMAP on the right. Figures by the Boomerang team [53] and WMAP Science Team [13]

The accuracy of the data from DASI, and to some extent from the 1-year WMAP as well, was not yet sufficiently high to provide good constraints on cosmological parameters. This situation has been improved in the 3- and 5-year data releases.

Currently there are only tentative measurements for the first few multipoles of the E-mode C_l^{E} and no detection for the B-mode C_l^{B} [13]. Only the spectra for the TE-crosscorrelation, C_l^{TE} is measured to some accuracy as can also be seen in the figure 4.2.

The data from WMAP is unarguably very good, but it is not perfect. The instrument does not have an infinitely small angular resolution but is limited to $l \lesssim 900$. Thus one can augment the WMAP data by including data from other, ground-based, experiments that probe the smaller scale anisotropies. In our analysis we include additional data from CBI [58] and ACBAR [59] in [2] and Boomerang [60] and ACBAR [59] in [3].

The problem with combining data from different instruments for the same observables, the CMB anisotropies in this case, brings up the question of calibration or some other systematic errors between the instruments. The best case would be that one instrument would provide the angular power spectra to small enough scales that there would be no need to add additional sources for the data. The Planck satellite by ESA [61] can hopefully provide just this. It is to be launched within a year and should provide accurate measurements upto $l \lesssim 2500$. Planck is also designed to measure the polarisation and should get good spectra for the E-mode and hopefully at least detect the B-mode as well.

Matter Power Spectrum

In addition to the CMB anisotropies we also use the data on the matter power spectrum. It constrains the amount of matter in the universe and helps breaking degeneracies between the cosmological parameters. The matter power spectrum comes from measuring the redshifts to a large number of galaxies around us, typically tens to hundreds of thousands of redshifts are measured. The article by the SDSS collaboration [62] discusses the constraints from the matter power spectrum extensively. In our analyses we use the SDSS data [62, 5].

The problem with the observed matter power spectrum is that on the smallest scales it probes, the evolution of the perturbations begins to be nonlinear. Thus one must either model the nonlinear evolution in the calculated matter power spectra in order to make comparisons with the data, or not use the smallest scale data at all. In our analysis we remain on the perturbative regime and do not consider the nonlinear structure.

4.2 Cosmological Parameters and the CMB Spectra

4.2.1 Anisotropy Overview

Looking at the overall shape of the temperature C_l-spectrum it is easy to discern three distinct features. The flat part at large scales, $l \lesssim 100$, the oscillating part at the smaller scales $l \gtrsim 100$, and the decreasing amplitude of the oscillations. While the exact shape of the C_l must be obtained by numerical calculation, the physics behind the various parts is easy to understand [45].

The almost featureless part of the spectrum describing the largest scales at $l \lesssim 100$ is called the Sachs-Wolfe–plateau. This part of the spectrum corresponds to the scales that were outside the horizon at the time of recombination. There are essentially no features in the spectrum as there were no causal physics affecting these scales. The rise of power at the very largest scales at $l \lesssim 20$ is due to the evolution in the gravitational potential along the line of sight from us to the surface of last scattering. This evolution is caused by the vacuum energy that begins to dominate the energy density and flattens the potential wells of the matter. The photons blueshift as they fall into the potential well but do not redshift as much as they climb out, resulting in an additional energy.

The smaller scales enter the horizon before recombination and for those scales there can be causal effects. Before recombination the baryons and photons form a tightly coupled fluid due to photons scattering from the charged particles. The dark matter does not interact with this and the inhomogeneities in the dark matter simply grow in time. The photons start falling into the gravitational wells formed by the matter inhomogeneities. However, at some point when the photon density gets high enough, the photon pressure becomes great enough to counteract the gravitational pull and the overdensity in the baryon-photon fluid begins to decrease. This way the baryon-photon fluid begins to oscillate under gravity and pressure working against one another.

The first peak in the C_l corresponds to a scale that entered the horizon just enough before recombination that the oscillation had time to reach maximal overdensity and we see strong structure

on this scale. The next peak is a mode that had reached the maximal overdensity and then the maximal underdensity. Even though it is the first trough in the oscillation, it is because the angular power spectrum is essentially a square of the oscillations, it shows up as a peak in C_l.

There is not a uniform set of peaks in the angular power spectrum. The odd peaks are somewhat higher than the even ones and there is an overall damping of the amplitude in the small scales. The difference in the peak heights is caused by the baryons. Increasing the number of baryons decreases the pressure of the baryon-photon fluid, thus decreasing the counterforce for gravity and reducing the underdensities a little. This shows up as alternating heights in the angular power spectrum.

The overall damping of the power is due to the diffusion of photons. As the photons scatter around they move in a random walk. The distance travelled by random walk is proportional to the square root of the total distance travelled. The total distance is the mean free path of the photon times the time travelled. The characteristic time scale is of course the Hubble time, thus we have

$$d_{\mathrm{diff}} \sim \sqrt{d_{\gamma\mathrm{mfp}} H^{-1}}. \tag{4.1}$$

Anisotropies on scales less than d_{diff} should be suppressed and this is exactly what we see in the angular power spectra.

4.2.2 Cosmological Parameters

In the end what we are aiming for is to use the data to constrain the values of the cosmological parameters. They can naturally be divided into three sets: background, perturbation and calibration parameters.

Background

These are the parameters that define the evolution of the background universe. They are the total energy density parameter Ω_{tot} and its constituents Ω_i, the Hubble parameter today H_0 and the dark energy equation of state parameter w. Obviously, the exact number of different parameters depends on the model in question. In the simplest flat model with cosmological constant, denoted as ΛCDM-model, three parameters is enough. These being the baryon and cold dark matter densities, Ω_{b} and Ω_{c}, and H_0.

Often the Hubble parameter is not used as a free parameter as it is not that well constrained by the data as can be seen in the distribution of figure 4.5. Instead one uses the physical density parameters $\omega_i = h^2\Omega_i$. Now giving Ω_Λ, ω_b and ω_c is sufficient to specify the simplest model.

The CMB data alone can not constrain the spatial curvature and even the 5-year WMAP papers do not give constrains to Ω_{tot} from CMB alone. This is because what is determined very accurately by the CMB is the position first acoustic peak, i.e., the angle of the sound horizon at the last scattering surface, which is the ratio $r_s(z_{\mathrm{rec}})/d_A(z_{\mathrm{rec}})$. The sound horizon at the recombination, $r_s(z_{\mathrm{rec}})$, only depends on the physical matter densities ω_m and ω_c, which are constrained by the relative heights of the acoustic peaks. The angular diameter distance depends on Ω_{tot}, Ω_m, w and h. Thus measuring

the location of the first peak, one gets a measurement for the angular diameter distance at one scale and from this it is not possible to constrain all of the parameters simultaneously.

An additional constraint on the value of the Hubble parameter, for which there is independent measurements from the Hubble Space Telescope key project [63] allows one to get a considerably tighter constraint for the curvature, $\Omega_{\rm tot} = 1.003^{+0.017}_{-0.013}$ [56].

We restrict ourselves to study the flat case only as the evidence points to that direction. In the context of inflation obtaining a closed universe requires a bit of fine tuning [64]. Also, from a practical point of view, the inclusion of non-flat models makes the analysis in our case computationally infeasible.

Since the first peak position is accurately determined by the data, it makes sense to use that as an independent parameter

$$\theta = \theta(\omega_b, \omega_c, h) \equiv 100 \times \frac{r_s(z_{\rm rec})}{d_A(z_{\rm rec})}. \tag{4.2}$$

Perturbation

In the simplest ΛCDM-model with adiabatic perturbations only, the perturbations are parametrised by one amplitude and one spectral index. To consider more complicated models more parameters are needed and as discussed in the previous section, we require three amplitudes and three spectral indices.

Calibration

These are the extra parameters that are required, but do not really belong to either of the earlier groups. The most relevant one here is the reionisation optical depth τ which gives the fraction of photons that have rescattered since the recombination. As discussed earlier, the polarisation is very sensitive to the ionisation history of the universe. When the universe becomes ionised again by the light from the first stars, it is once again possible to produce more polarisation via Thomson scattering. The measured polarisation places good limits on the optical depth, but provides little or no limits to other parametres. This can be seen by replacing the polarisation data in the data analysis by a prior constraint on τ which has only small effect on the results [65].

Another is the bias parameter b of matter power spectrum. It is the relation between the measured and the primordial matter power spectrum

$$P_{\rm gal}^{\rm SDSS}(k)|_{z_{\rm eff}\simeq 0.15} = b^2 P_{\rm m}(k)|_{z=0}. \tag{4.3}$$

The measured power spectrum comes from the measurements of galaxy distributions that are made on a range of different redshits and the result is given at some effective redshift $z_{\rm eff}$, for example, in [66] they use $z_{\rm eff} \simeq 0.15$. The theoretical matter power spectrum is, on the other hand, given as it is now, i.e. at redshift zero.

In our second paper we had the bias as a free parameter, but in the last one we analytically marginalise or integrate over it as described in [51, 67].

4.3 Bayesian Method

In our first paper [1], we used a simple "grid" to explore the parameter space. It is very simple to implement and parallelise to use in a multiprocessor computer. Seeing that the results looked promising and warranted a further research it was obvious that the old method was insufficient for exploring the parameter space in detail.

In the grid method, one simply chooses a set of values for each parameter in advance, calculates the theoretical spectra and compares these with the data for each parameter combination. This scales to the power of the number of parameters. For example, with ten parameters and ten values for each, which gives a very coarse grid, one has 10^{10} combinations. Grossly underestimating the time taken by the calculation for a single set of parameters to be one second, results in the total time required to scan the grid being 317 years. Obviously, a better method is called for.

Fortunately a better method exists in the form of Bayesian analysis [68] (see also [69, 51]). What we have is a set of cosmological parameters $\boldsymbol{\theta}$ the values for which we want to determine and the data $\mathcal{D}$ we are using. The quantity we wish to obtain is $p(\boldsymbol{\theta}|\mathcal{D})$, which is the posterior probability density function (PDF) for the parameters $\boldsymbol{\theta}$ given the data $\mathcal{D}$.

The Bayes' theorem states, that the PDF $p(\boldsymbol{\theta}|\mathcal{D})$ is

$$p(\boldsymbol{\theta}|\mathcal{D}) = \frac{p(\mathcal{D}|\boldsymbol{\theta})p(\boldsymbol{\theta})}{m(\mathcal{D})}, \tag{4.4}$$

where $m(\mathcal{D}) = \int d\boldsymbol{\theta} p(\mathcal{D}|\boldsymbol{\theta})p(\boldsymbol{\theta})$ is called the marginal PDF of $\mathcal{D}$ and can be taken as a normalisation constant as it it independent of $\boldsymbol{\theta}$. The function $p(\boldsymbol{\theta})$ is the prior PDF of the parameters and encodes all the information about the parameters before using the data $\mathcal{D}$. The remaining part, $p(\mathcal{D}|\boldsymbol{\theta})$, is the likelihood function which is the PDF for observations to produce $\mathcal{D}$ for a given $\boldsymbol{\theta}$ and encodes all the information we get for the parameters from the data.

The likelihood, often denoted by $\mathcal{L}$, for a given value of $\boldsymbol{\theta}$ can be obtained by calculating the theoretical angular power spectra and comparing this to the measured one, with

$$-2\ln\mathcal{L} = \sum_l \frac{(C_l^{\mathrm{th}} - C_l^{\mathrm{obs}})^2}{\sigma_l^2} = \chi^2, \tag{4.5}$$

where σ_l^2 is the error of the measurement. This form for the likelihood is not mandated by any means, and the WMAP team provide their own likelihood code [56, 70, 71] that they have optimised to fully utilise the WMAP data at the cost of greater computational complexity. In general the likelihood is constructed such that a model with better fit to the data has higher likelihood than model with a poorer fit.

What we want to find out are the single parameter θ_i posterior PDFs and to obtain those we must integrate over all other components

$$p(\theta_i|\mathcal{D}) = \int d\theta_1 \ldots d\theta_{i-1} d\theta_{i+1} \ldots d\theta_n p(\boldsymbol{\theta}|\mathcal{D}). \tag{4.6}$$

It would appear that we are no better off than we were with the grid method since calculating the above integral by directly sampling the posterior distribution means calculating the spectra and likelihood at all points in the parameter space.

Instead of sampling the posterior PDF directly, which clearly is computationally very intensive operation, we can sample the posterior by forming a Markov chain by the Metropolis-Hastings–algorithm [68] (and references therein). This method is called the Markov chain Monte Carlo (MCMC) method. This process generates a chain of correlated samples which, when the chain is run long enough, reaches an equilibrium at which point the samples can be regarded as samples from the posterior PDF. This method scales roughly linearly as the number of parameters is increased, thereby making it viable for studying more complicated models.

The Metropolis-Hastings–algorithm works with a very simple principle. When the Markov chain is at $\boldsymbol{\theta}_i$ in the parameter space a new location $\boldsymbol{\theta}'$ is generated by an auxiliary PDF $q(\boldsymbol{\theta}'|\boldsymbol{\theta}_i)$. The chain moves to this new location with propability $\alpha(\boldsymbol{\theta}'|\boldsymbol{\theta}_i)$ which is given by

$$\alpha(\boldsymbol{\theta}'|\boldsymbol{\theta}_i) = \min\left\{\frac{p(\boldsymbol{\theta}')p(\mathcal{D},\boldsymbol{\theta}')q(\boldsymbol{\theta}_i|\boldsymbol{\theta}')}{p(\boldsymbol{\theta}_i)p(\mathcal{D},\boldsymbol{\theta}_i)q(\boldsymbol{\theta}'|\boldsymbol{\theta}_i)}, 1\right\}, \tag{4.7}$$

with $p(\mathcal{D},\boldsymbol{\theta})$ being the Likelihood function. Commonly we have uniform or flat prior distribution $p(\boldsymbol{\theta}') = p(\boldsymbol{\theta}_i)$, i.e., we do not have any preferences for the values of parameters. Also the generating PDF is often symmetric $q(\boldsymbol{\theta}'|\boldsymbol{\theta}_i) = q(\boldsymbol{\theta}_i|\boldsymbol{\theta}')$ meaning that the new position in the chain is drawn from the same distribution in the whole parameter space. In this common case the transition propability reduces to a ratio between the likelihoods:

$$\alpha(\boldsymbol{\theta}'|\boldsymbol{\theta}_i) = \min\left\{\frac{p(\mathcal{D},\boldsymbol{\theta}')}{p(\mathcal{D},\boldsymbol{\theta}_i)}, 1\right\}. \tag{4.8}$$

Thus we generate the Markov chains by the MH-algorithm by choosing a random starting position at $\boldsymbol{\theta}_0$. Then we take the next trial step to $\boldsymbol{\theta}_1$ chosen from the generating PDF $q(\boldsymbol{\theta}_1|\boldsymbol{\theta}_0)$ and accept this with probability $\alpha(\boldsymbol{\theta}_1|\boldsymbol{\theta}_0)$. If the step is accepted we continue from $\boldsymbol{\theta}_1$ by the same process, if the step is rejected we take a new trial step from $\boldsymbol{\theta}_0$. In the abovementioned simple case when the transition probability is just the ratio between the likelihoods the new location if always chosen if the new set of parameters give a better fit to the data while a poorer fit is only occasionally chosen. This behaviour allows the chain to locate the global maximum of likelihood and scan the volume around it accurately. If the transition propability would not allow transitions to lower likelihood, the chain would easily be stuck at some local maximum.

An additional nice feature of the MCMC-method is that it is easy to parallelise by simply starting multiple chains. Since there is no, or very little, need to exchange information between the different chains, this kind of computation is exceptionally well suited for cluster computers.

As stated, the Markov chain does not immediately begin to sample the posterior PDF that we wish to uncover but there is a period called burn-in before the chain reaches equilibrium. While the theory quarantees that the chain will eventually reach the equilibrium, or converge, for a wide selection of generating PDFs it makes no claims about how long this will take. Also, there is no simple indicator to follow the convergence of the chain. In practice this means that one needs to keep an eye on the chains as they are generated.

One statistic to follow is the Gelman-Rubin $R-1$ statistic [72]. This does not measure the convergence of the chains, but their mixing instead. It means essentially that $R-1$ is around zero

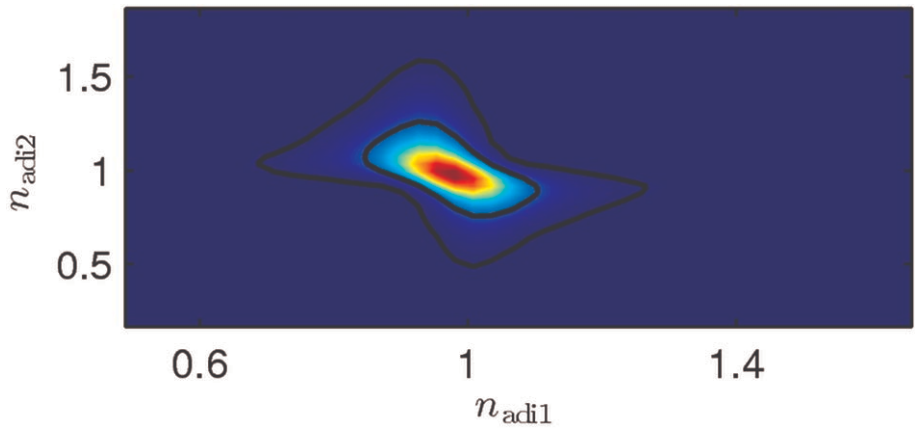

Figure 4.3: Two-dimensional distribution for the two adiabatic spectral indices. The effect when one index is more strictly constrained while the other is less strictly constrained is clearly visible.

if the chains have all scanned the same region in the parameter space. While this alone can not quarantee that the chains have really converged, looking at the chains themselves to see how they have covered the parameter space, one can be fairly certain the the results hold. Should one come across some pathological case where the parameter space has multiple distinct local likelihood maxima (multimodal parameter space), then using the MCMC-method would become problematic. This is not the case for the parameters we are analysing. For the simple adiabatic ΛCDM the likelihoods are nearly Gaussian and in our case somewhat distorted but still not multimodal, thus making the use of MCMC-method a valid approach.

4.3.1 The Choice of Parameters for the MCMC Runs

The best set of parameters is such that changing any one of them also affects the predictions, or, that there are no degeneracies between the parameters. An example of a degenerate pair is the adiabatic spectral index n and optical depth τ when considering the simple adiabatic model in absence of polarisation data. Increasing τ suppresses the angular power on small scales, but this can be compensated, up to a point, by increasing n. This degeneracy is no longer a problem since the optical depth is now accurately constrained by the polarisation data.

We are now considering a more complicated model and found there to be a problem with the standard parametrisation of the perturbations with spectral indices. The full angular power spectrum is

$$C_l = A^2[(1-\alpha)(1-|\gamma|)\hat{C}_l^{\mathrm{ad1}} + (1-\alpha)|\gamma|\hat{C}_l^{\mathrm{ad2}} + \alpha\hat{C}_l^{\mathrm{iso}} + \alpha_{\mathrm{cor}}\hat{C}_l^{\mathrm{cor}}], \tag{4.9}$$

where we defined a shorthand notation for the factor in the last term

$$\alpha_{\mathrm{cor}} = \mathrm{sign}(\gamma)\sqrt{\alpha(1-\alpha)|\gamma|}. \tag{4.10}$$

The total spectrum is dominantly adiabatic with a small fraction of isocurvature allowed. In terms of parameters this means that α is small. Now the problem is that when α is practically zero,

the isocurvature spectral index becomes essentially unconstrained. This is because the isocurvature spectral index only shows up in the isocurvature spectrum $\hat{C}_l^{\rm iso}$ and with $\alpha \approx 0$ it has no contribution to the total spectrum.

A similar case happens with the two adiabatic indices $n_{\rm ad1}$ and $n_{\rm ad2}$. Again with small α also the contribution from the correlation $\hat{C}_l^{\rm cor}$ is small and the degree of correlation, γ can vary freely. Now, when $|\gamma| \approx 0$ the contribution from $\hat{C}_l^{\rm ad2}$ is small and $n_{\rm ad2}$ becomes unconstrained and vice versa for $|\gamma| \approx 1$. This effect can be seen in the figure 4.3.

To alleviate this problem, instead of using an amplitude and a tilt, or a spectral index, to describe the perturbation spectra, we define two amplitudes at different scales instead. We choose to specify the amplitudes at scales $k_1 = 0.002\,{\rm Mpc}^{-1}$ and $k_2 = 0.05\,{\rm Mpc}^{-1}$. More details about the relation between these parametrisations see the appendix of [3]. Using this parametrisation the MCMC chains converge considerably faster than with the standard parametrisation.

Thus our final set of 10 parameters is

Background		Amplitude at k_1		Amplitude at k_2	
ω_b	physical baryon density	$\ln A_1^2$	overall	$\ln A_2^2$	overall
ω_c	physical cold dark matter density	α_1	isocurvature	α_2	isocurvature
τ	reionisation optical depth	γ_1	correlation	γ_2	correlation
θ	angle of the sound horizon				

These are out primary parameters for which we assign flat prior probability densities and all other parameters are derived from these.

4.4 Results

In this section we present select results and refer to the papers [1, 2, 3] for the full details.

4.4.1 Adiabatic Spectral Index

As discussed in the section 4.3.1 above, the adiabatic spectral indices are conditionally constrained. This can be seen in the one-dimensional distributions in figure 4.6 where the distributions for $n_{\rm ad1}$ and $n_{\rm ad2}$ are very wide. The two-dimensional distribution in figure 4.3 also clearly shows that when one index is close to unity, which is the expected value, the other can vary on a wide range.

When considering the adiabatic model, the spectral index n is very well constrained. Have we lost this accuracy with the introduction of the more compicated model? Fortunately this is not the case since comparing $n_{\rm ad1}$ and/or $n_{\rm ad2}$ to n means comparing wrong parameters. Since now our adiabatic spectrum is formed out of two parts, we can define an effective adiabatic spectral index as follows

$$n_{\rm ad}^{\rm eff}(\tilde{k}) - 1 = \frac{d\ln \mathcal{P}_{\mathcal{R}}(\tilde{k})}{d\ln k} = \frac{(n_{\rm ad1}-1)(1-|\gamma|)\tilde{(k)}^{n_{\rm ad1}-1} + (n_{\rm ad2}-1)|\gamma|\tilde{k}^{n_{\rm ad2}-1}}{(1-|\gamma|)\tilde{k}^{n_{\rm ad1}-1} + |\gamma|\tilde{k}^{n_{\rm ad2}-1}}. \qquad (4.11)$$

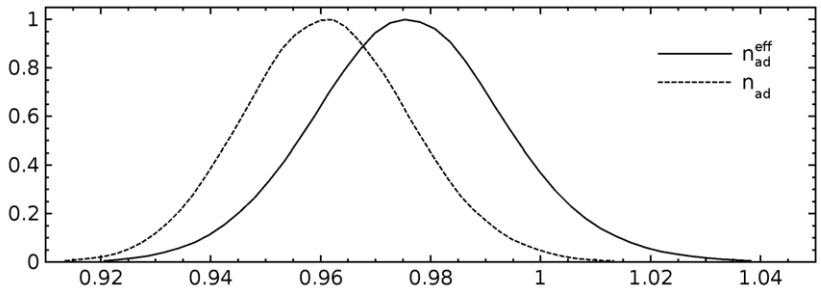

Figure 4.4: The effective adiabatic spectral index $n_{\rm ad}^{\rm eff}$ of our correlated model compared with the spectral index n of the pure adiabatic model.

Defined as such, the spectral index is a scale dependent quantity. To compare with the simple adiabatic spectral index we need $n_{\rm ad}^{\rm eff}$ at the pivot scale, i.e., when $\tilde{k} = 1$, which gives

$$n_{\rm ad}^{\rm eff}|_{k=k_0} = (n_{\rm ad1} - 1)(1 - |\gamma|) + (n_{\rm ad2} - 1)|\gamma| + 1. \tag{4.12}$$

Now comparing this effective spectral index $n_{\rm ad}^{\rm eff}$ to the simple adiabatic one n we see that the $n_{\rm ad}^{\rm eff}$ is also well constrained as is shown in figure 4.4.

4.4.2 Nonadiabatic Contribution

We show one-dimensional marginalised likelihoods for selected primary and derived parameters in figures 4.5 and 4.6. Instead of the amplitudes at k_1 and k_2 we show the derived parameters: the spectral indices and the amplitude parameters α and γ at the intermediate scale $k_0 = 0.01\text{Mpc}^{-1}$ since they are the more familiar parameters.

The data lead to likelihood peaks at clearly non-zero values for α (the ratio of the primordial entropy perturbation power to the total perturbation power at k_0) and favour a positive γ. (This significantly reduces the pivot-scale dependence of the likelihoods discussed in [2].) These are obtained from the likelihood functions corresponding to the amplitude parametrisation with flat priors for the primary parameters. As can be seen from figure 4.5 the exact confidence levels depend on the assumed priors, but the conclusions are not changed at a qualitative level. We discuss the priors more in section 4.4.4.

Since the definitions of the primary amplitude parameters (e.g. α) depend on the choice of pivot scale, we also define

$$\alpha_T \equiv \frac{\sum(2l+1)(C_l^{\rm iso} + C_l^{\rm cor})}{\sum(2l+1)C_l}\,, \tag{4.13}$$

the total non-adiabatic contribution to the CMB temperature variance,

$$\left\langle \left(\frac{\delta T}{T}\right)^2 \right\rangle = \sum_l \frac{2l+1}{4\pi} C_l\,. \tag{4.14}$$

One thing to note about α_T as defined above, is that it can be negative. This is because the correlation, which can be negative, is between the second adiabatic and the isocurvature parts, it can

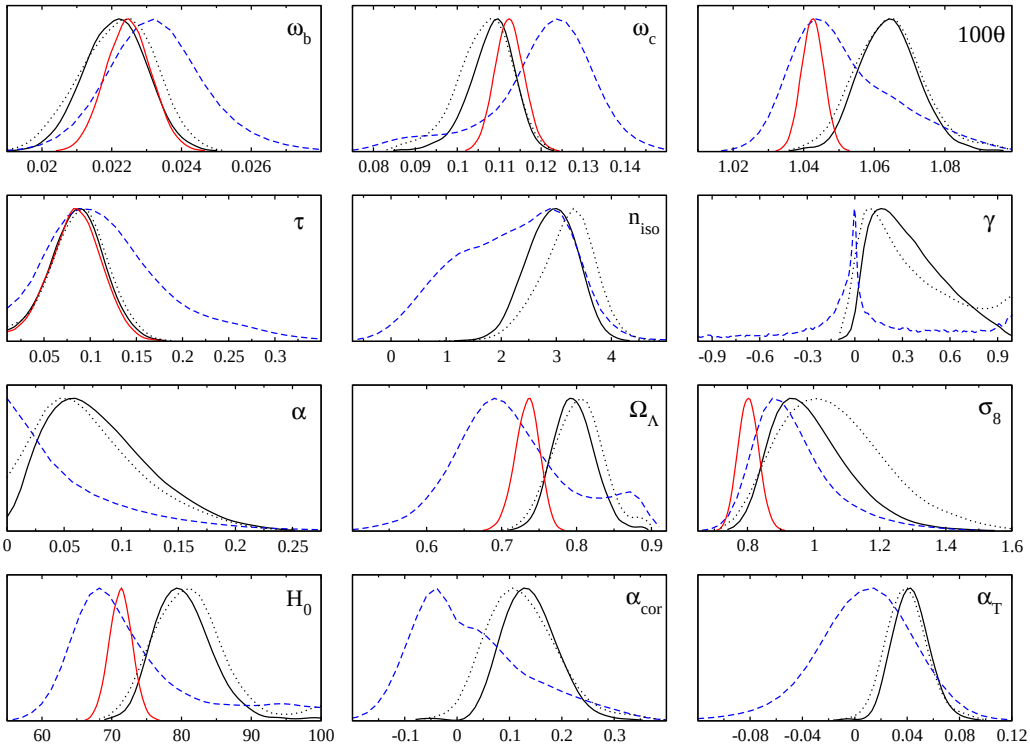

Figure 4.5: Marginalised likelihood functions for selected primary and derived parameters. The *solid black* curves are our new results for the correlated model. The *dotted black* curves show the effect of assigning flat priors in the index parametrisation instead of the amplitude parametrisation. The *red* curves are for an adiabatic model using the same data. The *dashed blue* curves are from our previous study [2] using data available in 2004. Note that also in the adiabatic model WMAP3 data favours a larger H_0 than WMAP1 (not shown)—allowing isocurvature modes favours larger H_0 regardless of which WMAP data set is used, although the effect is much stronger with WMAP3. Figure from [3].

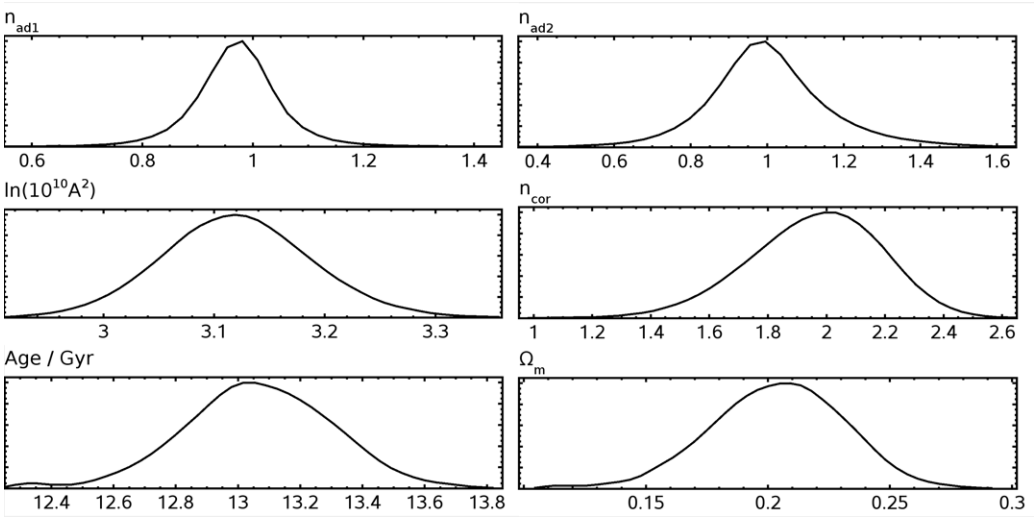

Figure 4.6: Marginalised likelihood functions for additional parameters not shown in figure 4.5. In this figure we only show the distributions for our the correlated model.

	ω_b	ω_c	100θ	τ	$n_{\rm ad1}$	$n_{\rm ad2}$	$n_{\rm iso}$	α	γ
A	0.0223	0.1066	1.062	0.0914	0.975	0.919	3.54	0.0539	0.180
B	0.0224	0.1124	1.042	0.0856	0.960				

	Ω_Λ	H_0	$\alpha_{\rm cor}$	α_T
A	0.800	80.3	0.096	0.0356
B	0.734	71.2		

Table 4.1: The best-fit models. A: The full model with a correlated isocurvature mode. B: The adiabatic model.

be larger than the isocurvature part thus making it possible for $C_l^{\rm iso} + C_l^{\rm cor} < 0$. The total angular power spectrum is naturally always positive or zero. We find $\alpha_T = 0.043 \pm 0.015$, and the whole 95% C.L. range $0.017 < \alpha_T < 0.073$ is positive. Thus it appears that the CMB data clearly favour a non-zero non-adiabatic contribution.

Our best-fit model and also the best-fit adiabatic model are given in table 4.1. They are compared in figure 4.7. The WMAP 3-year data prefer a slightly narrower $2^{\rm nd}$ peak than the adiabatic model can produce. This holds for the third peak also, but now the peak position and width are determined by the Boomerang data.

This feature in the data can be accounted for by a correlated isocurvature component. It can narrow down the $2^{\rm nd}$ peak without affecting the $1^{\rm st}$ peak position, which is accurately determined by the data. Increasing θ shifts the whole peak structure to the left while making the peaks narrower. Adding a positively correlated isocurvature component returns the $1^{\rm st}$ peak to its place. In figure 4.8 one clearly sees the correlation in the (α_T, θ)-pair as increasing the non-adiabatic part also θ increases.

Compared to the adiabatic model, adding 4 parameters improved the fit by $\Delta\chi^2 = 9.7$ from a total of $\Delta\chi^2 = 3608.78$. This comes mainly from the fit to the WMAP and Boomerang temperature $C_l^{\rm TT}$. At the $2^{\rm nd}$ peak for the WMAP data and at the $3^{\rm rd}$ peak for the Boomerang data. The data on the $C_l^{\rm TE}$ and $C_l^{\rm EE}$ are too inaccurate for a few per cent isocurvature contribution to play any role. Therefore the contribution to χ^2 from these cross-correlation data is the same for the adiabatic and our model. The fit to the SDSS data has improved slightly, whereas that to the ACBAR data is indifferent. In Table 4.2 we give quantitative numbers for the contributions of different data sets to the best-fit models. The best-fit model and its χ^2 with the data are of course not affected by the issue of priors, which affects only the likelihoods. For the first time in the history of CMB temperature anisotropy observations, adding the CDM (or baryon) isocurvature degree of freedom improves the fit to the data, and the likelihoods of isocurvature parameters peak at non-zero values.

The other major effect is that the correlated isocurvature model favours a smaller CDM density ω_c (also ω_b is down, but not as much). This effect can also been seen in the two-dimensional distribution of (θ, ω_c)-pair (the correlated model has a higher θ) in figure 4.8. This is due to the correlation component $C_l^{\rm cor}$, which raises the first and third peaks with respect to the second one, as seen in figure 4.7. The lower values of ω_m and ω_b compensate this by raising the second peak.

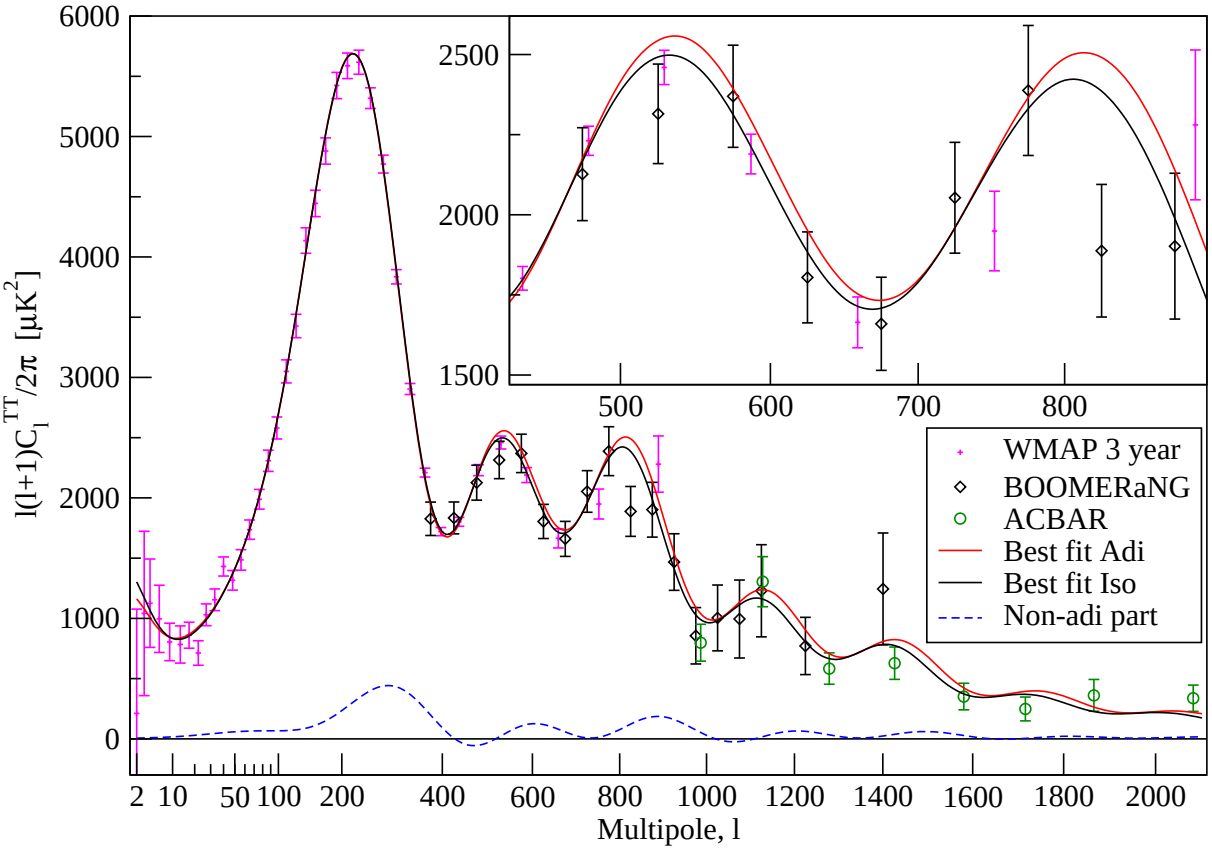

Figure 4.7: The CMB temperature angular power spectrum for our best-fit model (*black*) compared to the best-fit adiabatic model (*red*). The *dashed blue* curve shows the non-adiabatic contribution. The inset shows the 2nd and 3rd peaks. Figure from [3].

data set	χ^2 (A)	χ^2 (B)	$\Delta\chi^2$
WMAP	3535.20	3539.14	3.94
Boomerang	31.12	35.04	3.92
ACBAR	10.10	9.92	-0.18
SDSS LRG	22.64	24.66	2.02
total	3599.06	3608.78	9.72

Table 4.2: The χ^2 of the fit of the best-fit models to the data, and the contributions from the four different data sets. A: The full model with a correlated isocurvature mode. B: The adiabatic model.

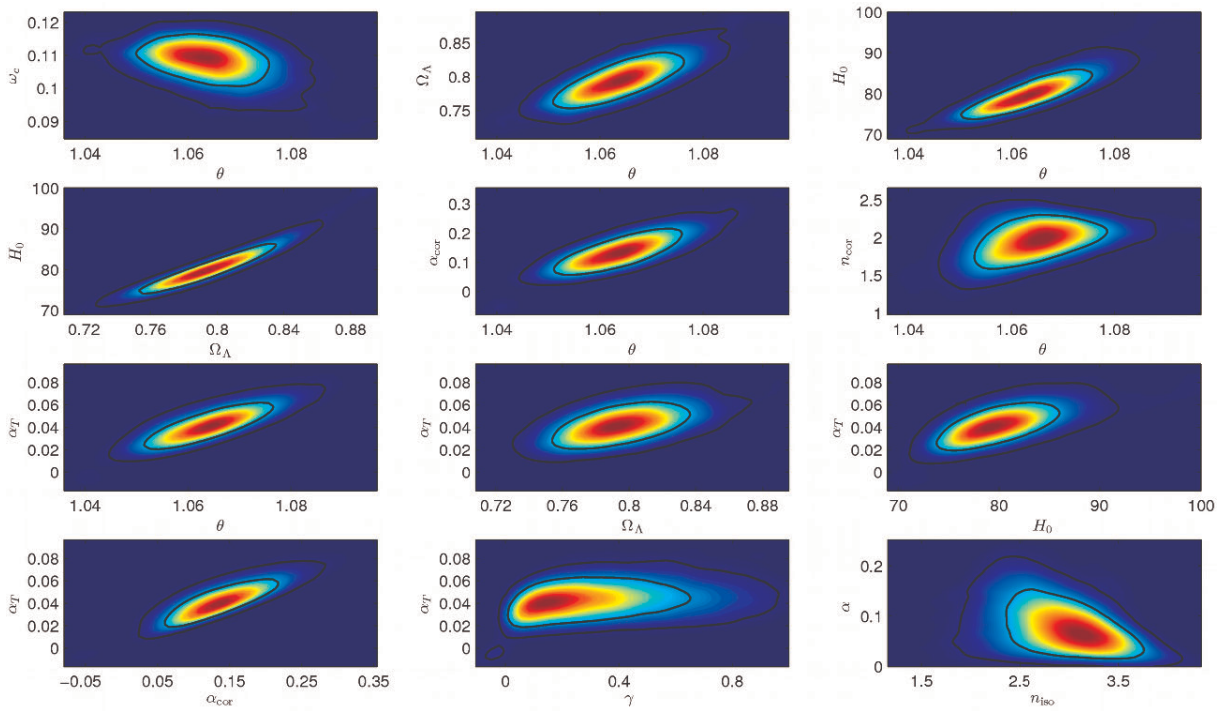

Figure 4.8: Select two-dimensional distributions. The correlations between the parameters are clearly visible, (H_0, θ), (Ω_Λ, H_0) and (θ, α_T) being the most obvious pairs.

For fixed ω_c and ω_b, increasing θ leads to a larger Ω_Λ and a larger Hubble constant H_0. For fixed θ and ω_b, a lower ω_c requires an even larger Ω_Λ and H_0. Therefore these models have a larger H_0 and a smaller matter density parameter $\Omega_m = 1 - \Omega_\Lambda$, than the adiabatic model.

4.4.3 Other Data Sets

In the non-adiabatic model we obtain large $h = 0.8 \pm 0.04$ and small $\Omega_m = 0.204 \pm 0.028$. This is not in line with other cosmological data. The Hubble Space Telescope has measured a value $h = 0.72 \pm 0.08$ [63] and estimates for Ω_m from supernovae give higher values than what we obtain. We assessed the effects of these data by postprocessing our chains and found that the significance of the non-adiabatic contribution decreases slightly.

More strict constraint comes from the Lyman-α data, which is an additional data on the smallest scales in the matter power spectrum. This data comes from observing the Lyman-α emissions from distant quasars [73]. This data can provide a strong constraint on $n_{\rm iso}$. Using the Lyman-α data as in [73] changes the distribution of α_T such that the peak is still clearly positive, but $\alpha_T = 0$ is now included in the 64% C.L. region. Since the Lyman-α data is at very small scales, including it to the analysis makes an implicit assumption that the power law approximation we made in (3.80) is valid for the whole k-range from the largest superhorizon scales to the Lyman-α scale.

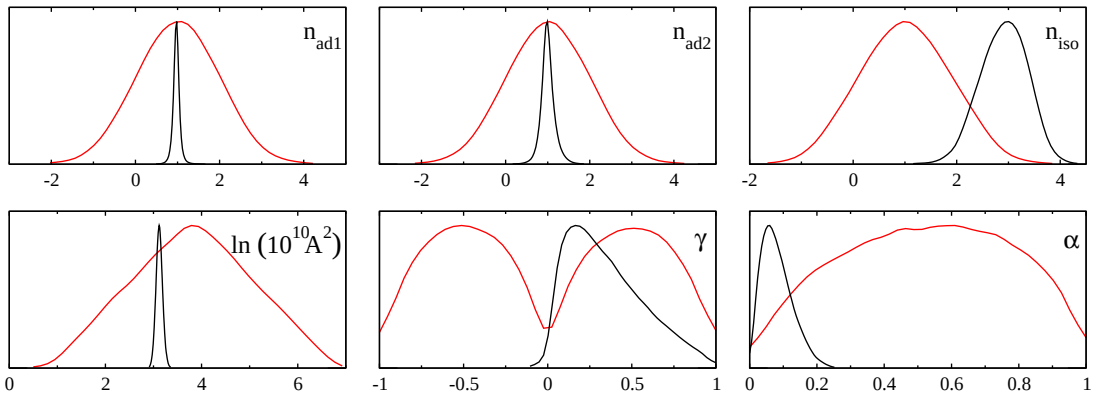

Figure 4.9: The *red* curves show the priors for the parameters of the index parametrisation, when flat priors are assumed for the parameters of the amplitude parametrisation. The *black* curves are the posterior likelihoods we have obtained (the same as the solid black curves in figure 4.5). Figure from [3].

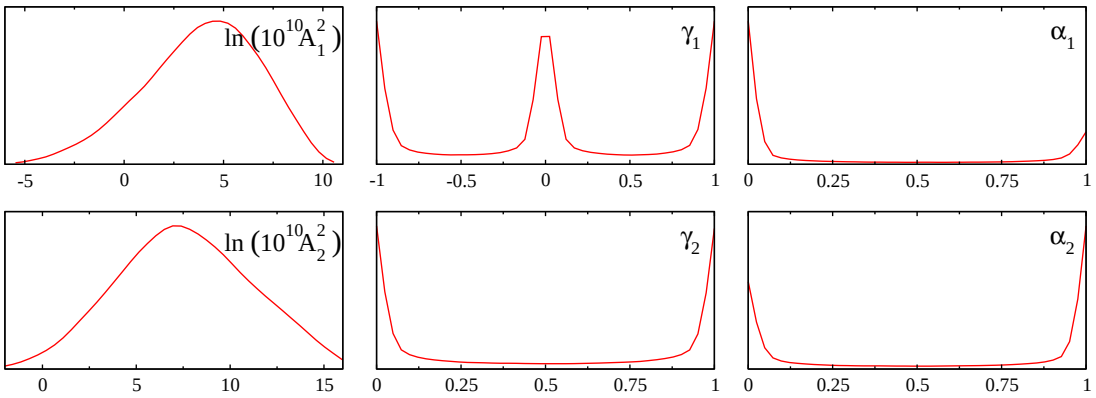

Figure 4.10: The priors for the parameters of the amplitude parametrisation, when flat priors are assumed for the parameters of the index parametrisation. Figure from [3].

4.4.4 The Issues with Priors

When some parameters of a model are not sufficiently tightly constrained by the data, the posterior likelihood functions become sensitive to the assumed prior probability densities for the parameters. Even when one assumes flat, i.e., uniform, priors for the primary parameters of the model, the question remains, which parameters are taken to be the primary parameters, since the priors for the quantities derived from the primary parameters (derived parameters) will not be flat. Since we chose the amplitudes at two different scales to be our primary parameters, it means the the priors for the spectral indices are not flat.

The mapping between the amplitude and spectral index parametrisations is presented in detail in [3]. In figures 4.9 and 4.10 we show what the priors of one parametrisation become when the priors of the other parametrisation are taken to be flat.

In the amplitude parametrisation the range of parameters (which is also a crucial part of the prior)

is throughout our study

$$\begin{aligned} \omega_b \in [0.005, 0.1], \quad & \omega_c \in [0.01, 0.99], \quad 100 \times \theta \in [0.3, 10.0], \quad \tau \in [0.01, 0.3] \\ \ln(10^{10} A_1^2) \in [1, 7], \quad & \alpha_1 \in [0, 1], \quad \gamma_1 \in [-1, 1] \\ \ln(10^{10} A_2^2) \in [1, 7], \quad & \alpha_2 \in [0, 1], \quad \gamma_2 \in [0, 1]\,. \end{aligned}$$

In the spectral index parametrisation the range of background parameters is the same as above, and the perturbation parameters have a uniform prior probability over the ranges

$$\begin{aligned} n_{\rm ad1} \in [-3, 4], \quad & n_{\rm ad2} \in [-3, 4], \quad n_{\rm iso} \in [-3, 12], \\ \ln(10^{10} A^2) \in [1, 7], \quad & \alpha \in [0, 1], \quad \gamma \in [-1, 1]\,. \end{aligned}$$

These are used only for producing figure 4.10, since all the analysis presented in [3] is based on MCMC runs in the amplitude parametrisation. However, we have checked against a MCMC run using the index parametrisation, that its results agree with the dotted black curves in figure. 4.5. For figure 4.10 we chose the above ranges of spectral indices to match this check run and our previous study [2]. As indices are not symmetric around the scale invariance ($n = 1$), we can see mild asymmetries in figure 4.10.

The parameters $\alpha_{\rm cor}$ and α_T are derived parameters and therefore their prior distributions are not flat in either parametrisation. We demonstrate the situation with $\alpha_{\rm cor}$ in figure 4.11. We see that $\alpha_{\rm cor}$ as well as the parameters $n_{\rm iso}$, γ, and α (see figure 4.9) are not well enough determined by the data to make their likelihood functions insensitive to the choice of priors. The solid blue curve in figure 4.11 is the ratio of the posterior and prior likelihoods for $\alpha_{\rm cor}$, and illustrates what the likelihood of $\alpha_{\rm cor}$ could be, if $\alpha_{\rm cor}$ had a flat prior probability density. The actual likelihood of course depends also on the other priors.

In figure 4.12 we show the prior and posterior distributions of α_T in the amplitude parametrisation. We see that the prior is relatively flat in the region where the posterior mostly lies. Consequently, unlike for $\alpha_{\rm cor}$ the ratio of posterior and prior likelihoods (posterior/prior) for α_T is almost indistinguishable from the posterior. Thus the situation with α_T is better in this respect than the case of $\alpha_{\rm cor}$, and the conclusions about α_T are more robust.

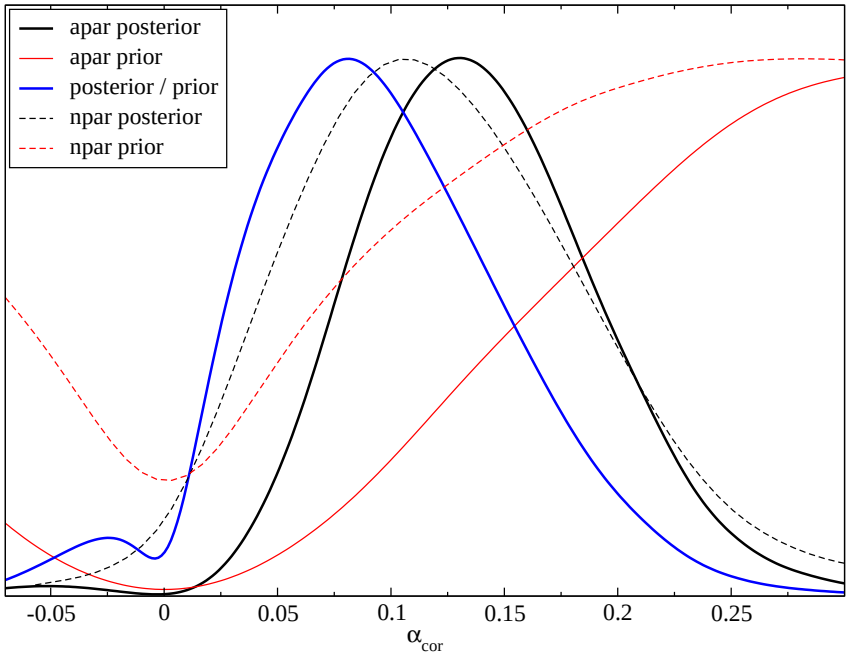

Figure 4.11: Prior and posterior likelihoods for the derived parameter $\alpha_{\rm cor}$. The *solid red* curve is the prior in the amplitude parametrisation and the *dashed red* curve is the same in the index parametrisation. The *solid* and *dashed black* curves are the corresponding posterior likelihoods. These are the same as the solid and dotted black curves in the $\alpha_{\rm cor}$ panel of figure 4.5. The *solid blue* curve is the ratio of the posterior and prior likelihoods in the amplitude parametrisation. Figure from [3].

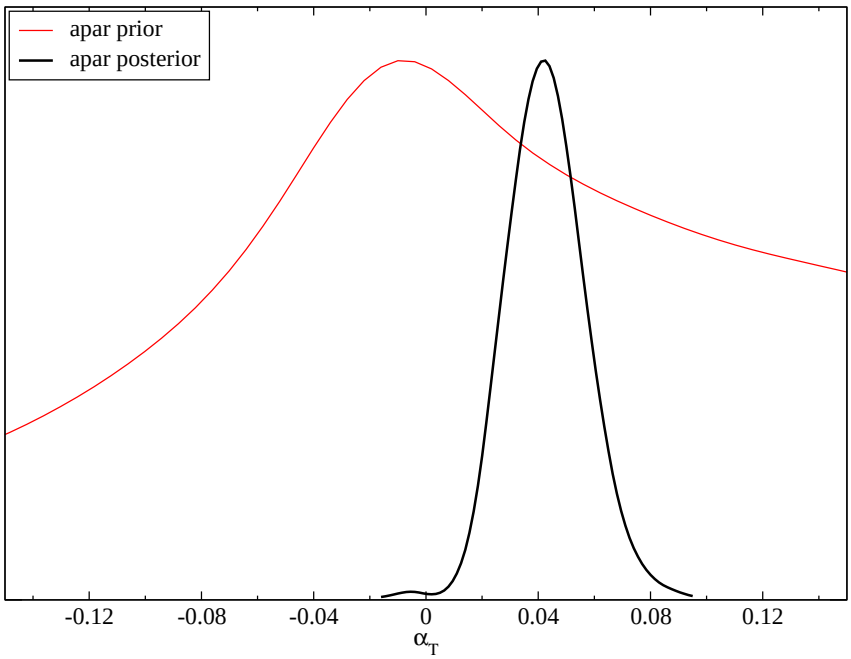

Figure 4.12: Prior *thin red* and posterior *thick black* likelihoods for the derived parameter α_T. Both likelihoods are for the amplitude parametrisation. Posterior/prior would be almost indistinguishable from the posterior. Figure from [3].

Chapter 5

Summary

In this thesis we have studied a slightly more complicated model producing the small anisotropies in the cosmic microwave background, namely, the possibility of an isocurvature component in addition to the usual adiabatic one. While the early, pre-3-year WMAP data allowed the possibility of such a component, they did not show any preference towards it. The slightly surprising result came from the WMAP 3-year data supplemented by the additional data from the ground-based Boomerang experiment which, for the first time, show a clear preference for a non-zero non-adiabatic component in the temperature anisotropies.

Perhaps the most interesting implication of this result is that in order to produce isocurvature perturbations in the early universe, one requires more complicated physics in the early universe. Currently, the paradigm of inflation is practically the only serious candidate for producing the perturbations in the energy density of the universe in the first place. The simplest models only have a single field but have been able to accommodate all the observations thus far. However, in order to produce isocurvature perturbations, the single field inflation fails and one needs to consider multi-field models.

In addition to just finding out this non-adiabatic component, we were able to indicate where it came from in the angular power spectra. The measured peak structure deviates slightly from the one predicted by the purely adiabatic perturbations and this small discrepancy can be corrected by the additional correlated isocurvature component. Additional and more accurate data on the CMB is being continually produced and this future data will show wheather or not this feature in the CMB will remain.

During these studies, we have improved our analytical methods used to study the CMB spectra. From the practical point of view, the most dramatic improvement came when switching the parametrisation of the perturbation power spectra from the spectral index parametrisation to the amplitude parametrisation. This considerably speeds up the generation of the Monte Carlo Markov chains and thus enhances the whole analysis.

On the observational front the most expected event must be the launch of the Planck satellite, hopefully in the near future. The data from Planck will provide us the CMB angular power spectra for temperature and polarisation in a wide range of multipoles, up to $l \lesssim 2500$, from a single instrument. This will reduce the possibility for various errors rising when combining data for the

same observable from different instruments. It will hopefully also act as a confirmation of the data from the WMAP satellite, for should both instruments produce similar results, where applicable, one can trust the results to be correct rather than an instrument glitch, uncleaned noise or some other non-cosmological signal.

Aside from the CMB measurements, there is a lot of activity on other observations as well. The matter power spectrum data will also improve as more and more galaxies are measured. Some other observables are also emerging, like the baryon acoustic oscillations [74] and the 21 cm emissions [75]. The baryon acoustic oscillations are the same oscillations as in the CMB, but now observed in the matter power spectrum, while the 21 cm emissions measure the emissions from the intergalactic medium which provides information, for example, on the matter power spectrum and reionisation.

All in all, there seems to be suggestions for more complicated physics that was previously required in the current data and no shortage of new data to test these suggestions against. It seems that for the cosmologists there are fruitful times ahead indeed.

References

[1] Jussi Valiviita and Vesa Muhonen. Correlated adiabatic and isocurvature cmb fluctuations in the wake of wmap. *Phys. Rev. Lett.*, 91:131302, 2003, astro-ph/0304175.

[2] Hannu Kurki-Suonio, Vesa Muhonen, and Jussi Valiviita. Correlated Primordial Perturbations in Light of CMB and LSS Data. *Phys. Rev.*, D71:063005, 2005, astro-ph/0412439.

[3] Reijo Keskitalo, Hannu Kurki-Suonio, Vesa Muhonen, and Jussi Valiviita. Hints of Isocurvature Perturbations in the Cosmic Microwave Background? *JCAP*, 0709:008, 2007, astro-ph/0611917.

[4] S. Perlmutter et al. Measurements of Omega and Lambda from 42 High-Redshift Supernovae. *Astrophys. J.*, 517:565–586, 1999, astro-ph/9812133.

[5] Max Tegmark et al. The 3d power spectrum of galaxies from the sdss. *Astrophys. J.*, 606:702–740, 2004, astro-ph/0310725.

[6] Douglas Clowe et al. A direct empirical proof of the existence of dark matter. *Astrophys. J.*, 648:L109–L113, 2006, astro-ph/0608407.

[7] Gianfranco Bertone, Dan Hooper, and Joseph Silk. Particle dark matter: Evidence, candidates and constraints. *Phys. Rept.*, 405:279–390, 2005, hep-ph/0404175.

[8] Edward W. Kolb and Michael S. Turner. *The Early Universe*. Addison-Wesley Publishing Company, 1990.

[9] O. Elgaroy et al. A new limit on the total neutrino mass from the 2dF galaxy redshift survey. *Phys. Rev. Lett.*, 89:061301, 2002, astro-ph/0204152.

[10] Subir Sarkar. Is the evidence for dark energy secure? *Gen. Rel. Grav.*, 40:269–284, 2008, 0710.5307.

[11] Teppo Mattsson. Dark energy as a mirage. 2007, 0711.4264.

[12] C.R. Benn and J.V. Wall. Structure on the largest scales: constraints from the isotropy of radio source counts. *Mon. Not. R. Astron. Soc.*, 272:678–698, 1995.

[13] G. Hinshaw et al. Five-Year Wilkinson Microwave Anisotropy Probe (WMAP) Observations:Data Processing, Sky Maps, & Basic Results. 2008, 0803.0732.

[14] Helge Kragh. *Cosmology and Controversy*. Princeton University Press, 1996.

[15] Gary Steigman. Primordial Nucleosynthesis in the Precision Cosmology Era. *Ann. Rev. Nucl. Part. Sci.*, 57:463–491, 2007, 0712.1100.

[16] J. Dunkley et al. Five-year wilkinson microwave anisotropy probe (wmap) observations: Likelihoods and parameters from the wmap data. 2008, 0803.0586.

[17] Keith A. Olive, Gary Steigman, and Terry P. Walker. Primordial nucleosynthesis: Theory and observations. *Phys. Rept.*, 333:389–407, 2000, astro-ph/9905320.

[18] F. de Felice and C.J.S Clarke. *Relativity on Curved Manifolds*. Cambridge University Press, 1990.

[19] Sean M. Carroll. *Spacetime and Geometry, An Introduction to General Relativity*. Addison Wesley, 2004.

[20] E. Komatsu et al. Five-Year Wilkinson Microwave Anisotropy Probe (WMAP) Observations:Cosmological Interpretation. 2008, 0803.0547.

[21] Alan H. Guth. The Inflationary Universe: A Possible Solution to the Horizon and Flatness Problems. *Phys. Rev.*, D23:347–356, 1981.

[22] Andreas Albrecht and Paul J. Steinhardt. Cosmology for Grand Unified Theories with Radiatively Induced Symmetry Breaking. *Phys. Rev. Lett.*, 48:1220–1223, 1982.

[23] Andrei D. Linde. Chaotic Inflation. *Phys. Lett.*, B129:177–181, 1983.

[24] Andrei D. Linde. Particle Physics and Inflationary Cosmology. 2005, hep-th/0503203.

[25] Andrew R Liddle and Samuel M Leach. How long before the end of inflation were observable perturbations produced? *Phys. Rev.*, D68:103503, 2003, astro-ph/0305263.

[26] Viatcheslav F. Mukhanov, H. A. Feldman, and Robert H. Brandenberger. Theory of cosmological perturbations. Part 1. Classical perturbations. Part 2. Quantum theory of perturbations. Part 3. Extensions. *Phys. Rept.*, 215:203–333, 1992.

[27] Hideo Kodama and Misao Sasaki. Cosmological Perturbation Theory. *Prog. Theor. Phys. Suppl.*, 78:1–166, 1984.

[28] Massimo Giovannini. Magnetized CMB anisotropies. *Class. Quant. Grav.*, 23:R1, 2006, astro-ph/0508544.

[29] Martin Bucher, Kavilan Moodley, and Neil Turok. The general primordial cosmic perturbation. *Phys. Rev.*, D62:083508, 2000, astro-ph/9904231.

[30] David H. Lyth, Karim A. Malik, and Misao Sasaki. A general proof of the conservation of the curvature perturbation. *JCAP*, 0505:004, 2005, astro-ph/0411220.

[31] N. Bartolo, E. Komatsu, Sabino Matarrese, and A. Riotto. Non-Gaussianity from inflation: Theory and observations. *Phys. Rept.*, 402:103–266, 2004, astro-ph/0406398.

[32] G. F. R. Ellis and M. Bruni. Covariant and Gauge Invariant Approach to Cosmological Density Fluctuations. *Phys. Rev.*, D40:1804–1818, 1989.

[33] David Langlois and Filippo Vernizzi. Evolution of non-linear cosmological perturbations. *Phys. Rev. Lett.*, 95:091303, 2005, astro-ph/0503416.

[34] Kari Enqvist, Janne Hogdahl, Sami Nurmi, and Filippo Vernizzi. A covariant generalization of cosmological perturbation theory. *Phys. Rev.*, D75:023515, 2007, gr-qc/0611020.

[35] Andrew R. Liddle and David H. Lyth. *Cosmological Inflation and Large-Scale Structure*. Cambridge University Press, 2000.

[36] David Langlois. Correlated adiabatic and isocurvature perturbations from double inflation. *Phys. Rev.*, D59:123512, 1999, astro-ph/9906080.

[37] David Langlois and Alain Riazuelo. Correlated mixtures of adiabatic and isocurvature cosmological perturbations. *Phys. Rev.*, D62:043504, 2000, astro-ph/9912497.

[38] Scott Dodelson. *Modern Cosmology*. Academic Press, 2003.

[39] Wayne Hu and Martin J. White. A CMB Polarization Primer. *New Astron.*, 2:323, 1997, astro-ph/9706147.

[40] Matias Zaldarriaga and Uros Seljak. An All-Sky Analysis of Polarization in the Microwave Background. *Phys. Rev.*, D55:1830–1840, 1997, astro-ph/9609170.

[41] Marc Kamionkowski, Arthur Kosowsky, and Albert Stebbins. Statistics of Cosmic Microwave Background Polarization. *Phys. Rev.*, D55:7368–7388, 1997, astro-ph/9611125.

[42] Marc Kamionkowski, Arthur Kosowsky, and Albert Stebbins. A probe of primordial gravity waves and vorticity. *Phys. Rev. Lett.*, 78:2058–2061, 1997, astro-ph/9609132.

[43] Uros Seljak and Matias Zaldarriaga. Signature of gravity waves in polarization of the microwave background. *Phys. Rev. Lett.*, 78:2054–2057, 1997, astro-ph/9609169.

[44] Matias Zaldarriaga and Uros Seljak. Gravitational Lensing Effect on Cosmic Microwave Background Polarization. *Phys. Rev.*, D58:023003, 1998, astro-ph/9803150.

[45] Wayne Hu and Scott Dodelson. Cosmic Microwave Background Anisotropies. *Ann. Rev. Astron. Astrophys.*, 40:171–216, 2002, astro-ph/0110414.

[46] Nicola Bartolo, Sabino Matarrese, and Antonio Riotto. CMB Anisotropies at Second Order I. *JCAP*, 0606:024, 2006, astro-ph/0604416.

[47] Nicola Bartolo, Sabino Matarrese, and Antonio Riotto. CMB Anisotropies at Second-Order II: Analytical Approach. *JCAP*, 0701:019, 2007, astro-ph/0610110.

[48] Uros Seljak and Matias Zaldarriaga. A line of sight approach to cosmic microwave background anisotropies. *Astrophys. J.*, 469:437–444, 1996, astro-ph/9603033.

[49] Michael Doran. CMBEASY:: an Object Oriented Code for the Cosmic Microwave Background. *JCAP*, 0510:011, 2005, astro-ph/0302138.

[50] Antony Lewis, Anthony Challinor, and Anthony Lasenby. Efficient Computation of CMB anisotropies in closed FRW models. *Astrophys. J.*, 538:473–476, 2000, astro-ph/9911177.

[51] Antony Lewis and Sarah Bridle. Cosmological parameters from CMB and other data: a Monte-Carlo approach. *Phys. Rev.*, D66:103511, 2002, astro-ph/0205436.

[52] George F. Smoot et al. Structure in the COBE differential microwave radiometer first year maps. *Astrophys. J.*, 396:L1–L5, 1992.

[53] P. de Bernardis et al. A Flat Universe from High-Resolution Maps of the Cosmic Microwave Background Radiation. *Nature*, 404:955–959, 2000, astro-ph/0004404.

[54] S. Hanany et al. MAXIMA-1: A Measurement of the Cosmic Microwave Background Anisotropy on angular scales of 10 arcminutes to 5 degrees. *Astrophys. J.*, 545:L5, 2000, astro-ph/0005123.

[55] C. L. Bennett et al. First Year Wilkinson Microwave Anisotropy Probe (WMAP) Observations: Preliminary Maps and Basic Results. *Astrophys. J. Suppl.*, 148:1, 2003, astro-ph/0302207.

[56] D. N. Spergel et al. Wilkinson Microwave Anisotropy Probe (WMAP) three year results: Implications for cosmology. *Astrophys. J. Suppl.*, 170:377, 2007, astro-ph/0603449.

[57] John Kovac et al. Detection of polarization in the cosmic microwave background using DASI. *Nature*, 420:772–787, 2002, astro-ph/0209478.

[58] A. C. S. Readhead et al. Extended Mosaic Observations with the Cosmic Background Imager. *Astrophys. J.*, 609:498–512, 2004, astro-ph/0402359.

[59] Chao-lin Kuo et al. High resolution observations of the cmb power spectrum with acbar. *Astrophys. J.*, 600:32–51, 2004, astro-ph/0212289.

[60] William C. Jones et al. A measurement of the angular power spectrum of the cmb temperature anisotropy from the 2003 flight of boomerang. *Astrophys. J.*, 647:823, 2006, astro-ph/0507494.

[61] http://sci.esa.int/planck/.

[62] Max Tegmark et al. Cosmological Constraints from the SDSS Luminous Red Galaxies. *Phys. Rev.*, D74:123507, 2006, astro-ph/0608632.

[63] W. L. Freedman et al. Final Results from the Hubble Space Telescope Key Project to Measure the Hubble Constant. *Astrophys. J.*, 553:47–72, 2001, astro-ph/0012376.

[64] Andrei Linde. Can we have inflation with Omega $>$ 1? *JCAP*, 0305:002, 2003, astro-ph/0303245.

[65] Antony Lewis. Observational constraints and cosmological parameters. 2006, astro-ph/0603753.

[66] Max Tegmark et al. Cosmological parameters from SDSS and WMAP. *Phys. Rev.*, D69:103501, 2004, astro-ph/0310723.

[67] S. L. Bridle et al. Analytic marginalization over CMB calibration and beam uncertainty. *Mon. Not. Roy. Astron. Soc.*, 335:1193, 2002, astro-ph/0112114.

[68] Nelson Christensen, Renate Meyer, Lloyd Knox, and Ben Luey. II: Bayesian Methods for Cosmological Parameter Estimation from Cosmic Microwave Background Measurements. *Class. Quant. Grav.*, 18:2677, 2001, astro-ph/0103134.

[69] Joanna Dunkley, Martin Bucher, Pedro G. Ferreira, Kavilan Moodley, and Constantinos Skordis. Fast and reliable MCMC for cosmological parameter estimation. *Mon. Not. Roy. Astron. Soc.*, 356:925–936, 2005, astro-ph/0405462.

[70] L. Page et al. Three year Wilkinson Microwave Anisotropy Probe (WMAP) observations: Polarization analysis. *Astrophys. J. Suppl.*, 170:335, 2007, astro-ph/0603450.

[71] G. Hinshaw et al. Three-year Wilkinson Microwave Anisotropy Probe (WMAP) observations: Temperature analysis. *Astrophys. J. Suppl.*, 170:288, 2007, astro-ph/0603451.

[72] A. Gelman and D. Rubin. Inference from iterative simulation using multiple sequences. *Statistical Science*, 7:457, 1992.

[73] Maria Beltran, Juan Garcia-Bellido, Julien Lesgourgues, and Matteo Viel. Squeezing the window on isocurvature modes with the Lyman- alpha forest. *Phys. Rev.*, D72:103515, 2005, astro-ph/0509209.

[74] Daniel J. Eisenstein et al. Detection of the Baryon Acoustic Peak in the Large-Scale Correlation Function of SDSS Luminous Red Galaxies. *Astrophys. J.*, 633:560–574, 2005, astro-ph/0501171.

[75] Steven Furlanetto, S. Peng Oh, and Frank Briggs. Cosmology at Low Frequencies: The 21 cm Transition and the High-Redshift Universe. *Phys. Rept.*, 433:181–301, 2006, astro-ph/0608032.